https://doi.org/10.5194/bg-2021-74
Preprint. Discussion started: 29 March 2021

Biogeosciences
Discussions
Open Access
EGU

Host influenced geochemical signature in the parasitic foraminifer *Hyrrokkin sarcophaga*

Nicolai Schleinkofer[1,2], David Evans[1,2], Max Wisshak[3]; Janina Vanessa Büscher[4,5], Jens Fiebig[1,2], André Freiwald[3], Sven Härter[1], Horst R. Marschall[1,2], Silke Voigt[1,2], Jacek Raddatz[1,2]

[1]Goethe Universität Frankfurt, Institut für Geowissenschaften, Frankfurt am Main, Germany

[2]Goethe Universität Frankfurt, Frankfurt Isotope and Element Research Center (FIERCE), Frankfurt am Main, Germany

[3]Senckenberg am Meer, Marine Research Department, Wilhelmshaven, Germany

[4]National University of Ireland Galway, Department of Earth and Ocean Sciences, Galway, Ireland

[5]GEOMAR Helmholtz Centre for Ocean Research Kiel, Department of Biological Oceanography, Kiel, Germany

Corresponding Author: Nicolai Schleinkofer (schleinkofer@em.uni-frankfurt.de)

Abstract

Hyrrokkin sarcophaga is a parasitic foraminifer that is commonly found in cold-water coral reefs where it infests the file clam *Acesta excavata* and the scleractinian coral *Lophelia pertusa*. Here, we present measurements of the elemental and isotopic composition of this parasitic foraminifer for the first time, analyzed by inductively coupled optical emission spectrometry (ICP-OES), electron probe micro analysis (EPMA) and mass spectrometry (MS).

Our results reveal that the geochemical signature of *H. sarcophaga* depends on the host organism it infests. Sr/Ca ratios are 1.1 mmol mol^{-1} higher in *H. sarcophaga* that infest *L. pertusa*, which could be an indication that dissolved host carbonate material is utilised in shell calcification, given that the aragonite of *L. pertusa* has a naturally higher Sr concentration compared to the calcite of *A. excavata*. Similarly, we measure 3.1 ‰ lower $\delta^{13}C$ and 0.25 ‰ lower $\delta^{18}O$ values in *H. sarcophaga* that lived on *L. pertusa*, which might be caused by the direct uptake of the host's carbonate material with a more negative isotopic composition or different pH regimes in these foraminifera (pH can exert a control on the extent of CO_2 hydration/hydroxylation) due to the uptake of body fluids of the host. We also observe higher Mn/Ca ratios in foraminifers that lived on *A. excavata* but did not penetrate the host shell compared to specimen that penetrated the shell, which could be interpreted as a change in food source, changes in the calcification rate, Rayleigh fractionation or changing oxygen conditions.

While our measurements provide an interesting insight into the calcification process of this unusual foraminifer, these data also indicate that the geochemistry of this parasitic foraminifer is unlikely to be a reliable indicator of paleoenvironmental conditions using Sr/Ca, Mn/Ca, $\delta^{18}O$ or $\delta^{13}C$ unless the host organism is known and its geochemical composition can be accounted for.

https://doi.org/10.5194/bg-2021-74
Preprint. Discussion started: 29 March 2021


Biogeosciences
Discussions
Open Access
EGU

1. Introduction

Foraminifera are a very diverse group of marine shelly organisms that are commonly used for paleoenvironmental reconstructions using the isotopic or elemental composition that is recorded in their carbonate shell (Costa et al., 2016; Gray and Evans, 2019; Sen Gupta, 2003; Hönisch et al., 2011; Lear and Rosenthal, 2006; Petersen et al., 2018; Raddatz et al., 2017). They first appeared in the Cambrian and, over the course of the Phanerozoic, occupied oceanic settings from coastal waters to the open ocean, as well as the benthic habitats of the deep sea (Goldstein, 1999). Multiple feeding methods are known from foraminifera, including suspension feeding, grazing, predation and parasitism (Hancock et al., 2015). The latter is probably the least common feeding mechanism among the foraminifera with only nine species that are known to be parasitic and a further 13 that are suspected to be (Walker et al., 2017). One of the known parasitic species is *Hyrrokkin sarcophaga* (Cedhagen, 1994), a common foraminifera in cold-water coral reefs in the NE-Atlantic (Beuck et al., 2008). *H. sarcophaga* preferentially colonises the file clam *Acesta excavata*, but also other organisms such as the bivalve *Delectopecten vitreus*, sponges of the family Geodiidae and Ancorinidae, cold-water corals such as *Lophelia pertusa, Madrepora occulata* and *Flabellum japonicum,* as well as other foraminifera (Beuck et al., 2008; Cheng and Dai, 2016). Besides biogenic hardgrounds, *H. sarcophaga* can also be found settling on rocks which shows that it can at least survive short periods without a host (Cedhagen, 1994). *H. sarcophaga* forms an attachment etching, i.e. mirroring its outline on the host. From this depression the foraminifer bores a canal into the shell of the host (Cedhagen, 1994)(Fig. 1) . This allows the foraminifera to feed on the host tissue (Cedhagen, 1994) and possibly assimilate amino acids from the calcifying fluid (Alexander and Delaca, 1987; Schweizer et al., 2012).

https://doi.org/10.5194/bg-2021-74
Preprint. Discussion started: 29 March 2021

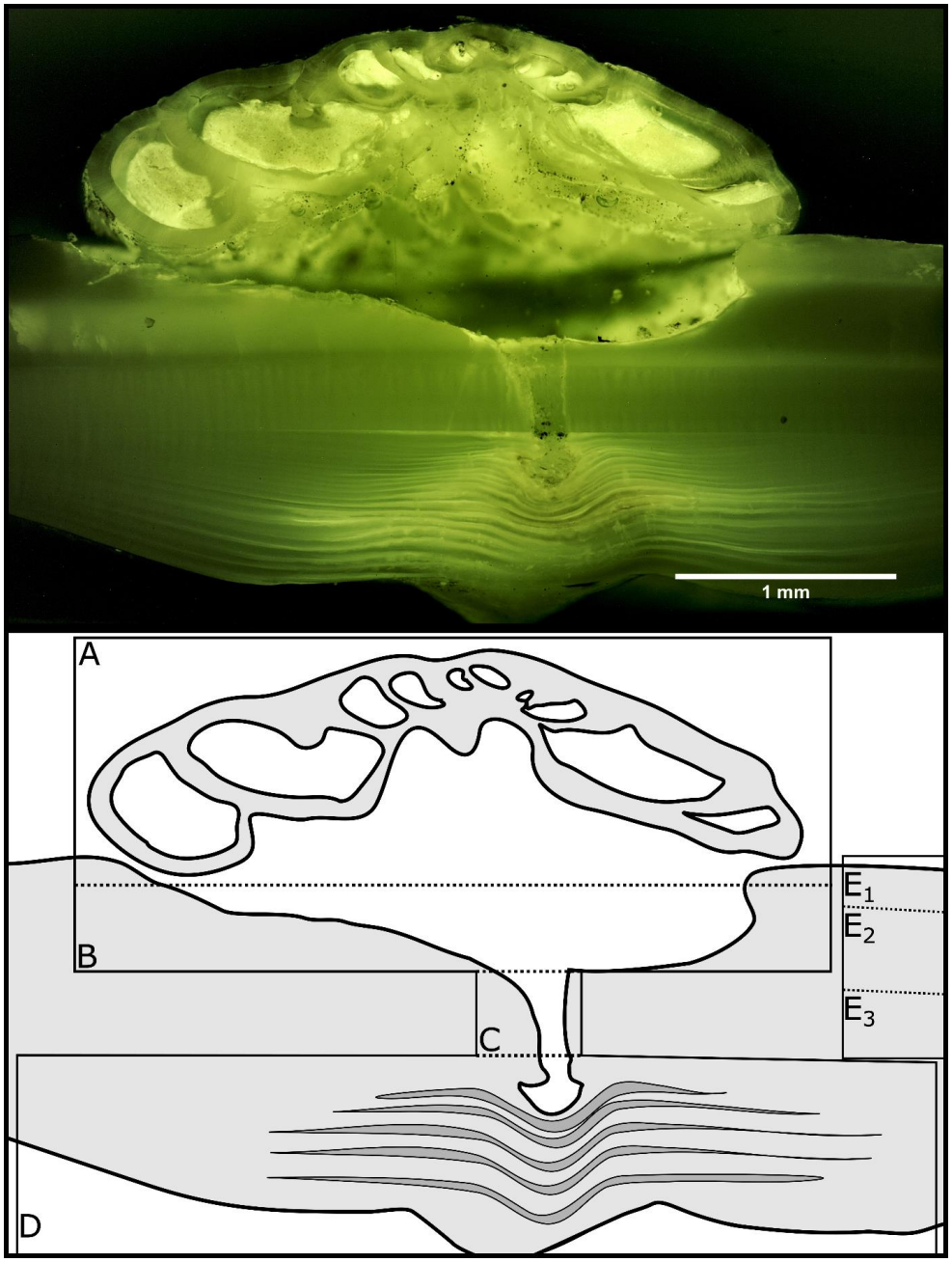

Figure 1 Fluorescence microscopic image (excitation 420 – 490 nm) and schematic figure of *H. sarcophaga* on *A. excavata*. A: *H. sarcophaga*, B: Attachment depression corroded by *H. sarcophaga*, C: Bored canal, D: Callus built by *A. excavata* (SRZ), E: Undisturbed shell, E_1: Calcitic shell layer (fibrous), E_2: Calcitic shell layer (microgranular), E_3: Aragonitic shell layer

https://doi.org/10.5194/bg-2021-74
Preprint. Discussion started: 29 March 2021

A. excavata reacts by building a callus to seal this boring (Fig 1D). This callus is a layered formation of aragonite rich in organic material that seals the boring of *H. sarcophaga* to defend the organism from the parasite's attack (Beuck et al., 2008). In *L. pertusa*, borings into the inner calyx area were not observed (Beuck et al., 2008). Instead multiple "whip"-shaped filaments protrude into the corals skeleton, which probably serve an anchoring function (Beuck et al., 2008). The pit is possibly formed either as a way to protect itself from cleaning attempts of the host and increase attachment strength or to satisfy calcium requirements in order to calcify (Beuck et al., 2008; Cedhagen, 1994).

As the parasitic foraminifera ingests material from its host, the question arises whether this process exerts an influence on the shell geochemistry of the parasite. Should this be the case, this factor may need to be accounted for, especially as some parasitic foraminifera, such as *Cibicides refulgens,* are also used in geochemical studies for paleoenvironmental reconstructions (Alexander and Delaca, 1987; García-Gallardo et al., 2017; Mackensen and Nam, 2014; Raddatz et al., 2011; Rathburn and De Deckker, 1997). If the geochemistry of the foraminifera shell depends systematically on the type of host that is infected, and these effects remain unknown, this could lead to erroneous palaeoenvironmental reconstructions. As far as we are aware, no previous studies have been conducted to test for this effect of different hosts on the geochemical composition of parasitic foraminifera.

Here we present element to Ca ratios (Mg/Ca, Sr/Ca, Na/Ca and Mn/Ca) and stable isotope data (oxygen and carbon) measured in *H. sarcophaga* collected from different host organisms (*A. excavata* and *L. pertusa*) from the Trondheimsfjord (Norway) to explore if and how the different hosts influence the geochemical composition of the foraminifera shell. In addition, we present element maps measured by electron microprobe analysis (EPMA) of the callus region of *A. excavata* in order to explore geochemical differences between the callus region and undisturbed shell areas.

2. Material and Methods

2.1. Sampling

All investigated samples were collected in the Leksa Reef, located at the entrance to the Trondheimsfjord in Norway (N 63.613056/E 9.384167, depth ~ 200 m) by means of the manned submersible JAGO (Hissmann and Schauer, 2017) during the scientific cruises POS473 and POS525 with R/V POSEIDON (Büscher, 2018; Form et al., 2015; Lackschewitz and Heinitz, 2015). In total we measured 28 specimen of *H. sarcophaga*, which were divided into three groups: 1. *H. sarcophaga* that infested *A. excavata* with callus formation (henceforth called HAW), 2. *H. sarcophaga* that infested *A. excavata* without callus formation (henceforth called HAO, HAW + HAO = HA), 3. *H. sarcophaga* that infested *L. pertusa* (henceforth called HL). Samples of *A. excavata* and *L. pertusa* were picked alive. For

https://doi.org/10.5194/bg-2021-74
Preprint. Discussion started: 29 March 2021

H. sarcophaga we cannot be entirely certain that they were still alive when sampled, however, when dead they are easily removed from the shell. Therefore, in case the foraminifera were dead when sampled, they died close to the time of sampling.

For electron probe micro analysis (EPMA) we used two samples of *A. excavata* with attached *H. sarcophaga*. The area of interest was cut from the shell with a handheld drilling tool, mounted vertically into circular mounts and embedded in epoxy resin. The sample surface was ground with 9 µm grid with silicon carbide sanding paper and then polished using 3 µm diamond-water based lapping paste.

For stable isotope measurements we used nine HAW, nine HAO and ten HL. The samples were ultrasonically rinsed in deionised water for five minutes and allowed to dry. Afterwards the samples were crushed in an agate mortar. About 100 µg of sample powder was transferred to borosilicate glass tubes and sealed with plastic caps.

For ICP-OES measurements we used ten HAW, ten HAO and ten HL samples. The samples were ultrasonically rinsed in deionised water for five minutes and allowed to dry. Afterwards the samples were crushed in an agate mortar. About 120 µg of sample powder was transferred to Eppendorf tubes and sealed.

Bivalve and coral samples were treated similarly to foraminifera samples. For stable isotopes and E/Ca analysis we used three shells. We took 15 - 20 samples per shell from the outermost shell section along the main growth axis, starting at the ventral margin. The corals were sampled randomly over the whole calyx area.

The manganese concentration of *L. pertusa* had to be determined by ICP-MS because it was below the limit of detection by ICP-OES. We used three specimens (two from the Leksa Reef, one from the Sula Reef) of which we sampled 150 µg from the fibrous shell section.

Samples of the ambient water were collected during scientific cruise POS525 with R/V POSEIDON in July 2018 (Büscher, 2018; Lackschewitz and Heinitz, 2015). A Rosette Sampler equipped with conductivity, temperature and depth sensors (CTD) was used to sample water from the investigated reefs. The water samples were transferred from 12 L Niskin bottles to 250 mL borosilicate bottles and sealed after adding 100 µL $HgCl_2$ to prevent biological activity of microorganisms that may alter the isotopic composition. The samples were stored in a fridge at 4 °C until measurement.

2.2. Shell carbonate polymorph

The polymorph of the foraminiferal shell was determined using cobalt nitrate solution (Meigen solution). The foraminifera samples were crushed in an agate mortar and transferred to Eppendorf

https://doi.org/10.5194/bg-2021-74
Preprint. Discussion started: 29 March 2021

containers. The samples were mixed with 10 w% $Co(NO_3)_2$ aqueous solution and allowed to react at 95°C for 20 minutes. Afterwards the samples were washed four times with MilliQ Water and inspected under a Microscope. Aragonite stains purple/pink in cobalt nitrate solution, whereas calcite is unaffected (Kato et al., 2003)

2.3. Fluorescence microscopy

We used fluorescence microscopy to investigate the distribution of the organic material in the foraminifera and the underlying bivalve shell. Fluorescent images were taken using a Leica DMRX-POL microscope with fluorescent front light and a 50 W mercury lamp. The microscope was equipped with an H3 filter cube, which excites in the wavelength range of blue to violet (Bandpass filter: 420 – 490 nm) The pictures were taken with a digital camera connected to the microscope with 0.25 s exposure time.

2.4. EPMA

Electron probe micro analyses were conducted at Goethe Universität Frankfurt on a JEOL JXA-8530F Plus Field Emission Gun Electron Probe Micro Analyzer (FEG-EPMA). Analysis conditions were: 15 kV acceleration voltage, 20 nA current with a beam diameter of 3 µm. We used TAP crystal for Mg, TAPL for Na and Sr and PETH for S. Detection limits are calculated with the equation given in Goldstein et al., 2017 and amount to: Mg = 178 µg g^{-1} (Mg/Ca = 0.7 mmol mol^{-1}), Na = 170 µg g^{-1} (Na/Ca = 0.7 mmol mol^{-1}), Sr = 129 µg g^{-1} (Sr/Ca = 0.1 mmol mol^{-1}), S = 152 µg g^{-1} (S/Ca = 0.4 mmol mol^{-1}) and Ca = 195 µg g^{-1}. The chemical maps were recorded with a beam diameter of 2 µm, 15 kV acceleration voltage and 20 nA current.

Molar ratios were calculated from the weight fractions of the specific oxides (CaO, MgO, Na_2O, SrO, SO_3) by calculating the concentration of the observed elements (in µg/g) and normalization to Ca.

2.5. ICP-OES

Elemental ratios Mg/Ca, Sr/Ca, Na/Ca and Mn/Ca (only for foraminifera and bivalves) were analyzed by inductively coupled plasma-optical emission spectrometry (ICP-OES). The ICP-OES analysis was carried out with Thermoscientific iCap 6300 Duo at the Institute of Geosciences, Goethe Universität Frankfurt. The sample powder (≈ 140 µg) was dissolved in 500 µL HNO_3 (2 %) and 300 µL aliquots were separated. Subsequently 1500 µL of 1.2 mg L^{-1} yttrium solution was added to each aliquot as an internal standard resulting in 1mg L^{-1}. The intensity data were background subtracted and standardized internally to Y and normalized to Ca. The reproducibility of the USGS MACS-3 and JCP1 carbonate reference material (n = 5)(Jochum et al., 2005) was better than 3% (relative standard deviation; % RSD) for Mg/Ca, Na/Ca, Sr/Ca and Mn/Ca.

https://doi.org/10.5194/bg-2021-74
Preprint. Discussion started: 29 March 2021

155 **2.6. ICP-MS**

156 For solution based ICP-MS measurements we used 150 µg of sample powder and dissolved it in 500 µL
157 2% HNO_3. The dissolved sample (300 µL) was mixed with 1500 µL 1.2 mg L^{-1} Yttrium solution which was
158 used as the internal standard. The reference material ECRM 752 (Greaves et al., 2008) was used to
159 monitor measurement precision. The reproducibility of the ECRM 752 carbonate reference material
160 (n= 3) was better than 1% for Mn/Ca

161 **2.7. Stable oxygen and carbon isotopes**

162 Stable isotopes were measured at Goethe Universität Frankfurt on a Thermo MAT 253 Mass
163 Spectrometer interfaced with a Thermo Fisher Scientific GasBench II. The sample material (100 µg) was
164 reacted with 99% H_3PO_4 at 72°C in continuous flow mode. Analytical procedures followed Spötl and
165 Vennemann (2003). $\delta^{13}C$ and $\delta^{18}O$ values are reported in δ-notation, i.e. ‰-deviation relative to Vienna
166 Pee Dee Belemnite (VPDB) and Vienna Standard Mean Ocean (VSMOW), respectively. Internal
167 precision is better than 0.06 ‰ ($\delta^{13}C$) and 0.08 ‰ ($\delta^{18}O$).

168 Water samples were analyzed for their isotopic composition at Friedrich-Alexander Universität
169 Erlangen-Nürnberg by an automated equilibration unit (Gasbench II; Thermo Fisher Scientific) coupled
170 in continuous flow mode to a Delta *plus* XP isotope ratio mass spectrometer (Thermo Fisher Scientific,
171 Bremen, Germany).

172 Water for $\delta^{13}C$ analyses was extracted from the sample bottles by a 1-mL disposable syringe through
173 the septa without opening the bottle to avoid loss of CO_2 during sample transfer. During water
174 extraction, the removed volume was simultaneously replaced by inert gas through a second needle
175 connected to an argon-filled gas sampling bag (Grace, Deerfield, IL, USA). The samples were injected
176 into 12 mL Labco Exetainers™ (Labco Ltd. Lampeter, U.K) that were prepared with phosphoric acid and
177 pre-flushed with helium (purity 99.999%). For seawater the injection volume was 0.85 mL per vial.
178 Samples were analyzed in duplicates and the reported values are arithmetic means. All values are
179 reported in the standard δ-notation in per mille (‰) vs. VPDB.

180 Sample bottles for $\delta^{18}O$ were de-capped and 0.5 mL water were extracted with a pipette for CO_2
181 equilibration. The samples were transferred into 12 mL Labco Exetainers™ (Labco Ltd. Lampeter, U.K)
182 and subsequently flushed with 0.3% CO_2 in helium. Equilibration time was 24 hours at 25 °C. All samples
183 were measured in duplicates and the reported values are arithmetic means. All values are reported in
184 the standard δ-notation in per mille (‰) vs. VSMOW. External reproducibility based on repeated
185 analysis of control samples was better than 0.1‰ and 0.05 ‰ for $\delta^{13}C$ and $\delta^{18}O$, respectively.

186 **2.8. Statistical computation**

https://doi.org/10.5194/bg-2021-74
Preprint. Discussion started: 29 March 2021

We used one way ANOVA to test the effect of the host species on the elemental and isotopic composition in *H. sarcophaga*. Shapiro-Wilk test and Levene's test were used to ensure normal distribution and equal variance of the target variables. Most groups and target variables are normally distributed except for Na/Ca in the HAO group and $\delta^{18}O$ in the HL group. All target variables except for Mn/Ca and Sr/Ca show equal variance based on the Levene's test. Normal distribution and equal variance are considered a prerequisite for ANOVA. As these prerequisites are not met in some groups we additionally tested the data with a Kruskal-Wallis test which can be regarded as a non-parametric alternative to ANOVA (Lantz, 2013). R scripts are available from the corresponding author.

3. Results

3.1. Carbonate Polymorph

The investigated *H. sarcophaga* samples show no staining (Supplement S2) under the influence of cobalt nitrate solution. Consequently the shells are built of calcite like other species of the order Rotaliida (Horton et al., 2021).

3.2. Fluorescence microscopy

The fluorescence microscopic image (Fig. 1) shows distinct fluorescent and non-fluorescent layers in the shell repair zone (SRZ) of the bivalve. Highly fluorescent material is also observable on *H. sarcophaga*, especially in the foramen.

The SRZ has a maximum thickness of 900 µm, decreasing in all directions. The fluorescent layers in the SRZ are 20 – 40 µm thick. These layers taper off distally from the bore canal and disappear. Non-fluorescent layers are generally smaller ranging from 9- 20 µm. The asymmetric pit that is produced by the foraminifera is observable, one side of the pit is rising steeply whereas the other side has a shallower angle. The bore canal, which starts at the bottom of the attachment etching, is 400 µm long in the undisturbed bivalve shell, but continues in the callus by another 240 µm. At the start of the bore the canal is 340 µm in diameter and continuously narrows to 140 µm. The canal ends in the SRZ with a "mushroom-like" shape.

https://doi.org/10.5194/bg-2021-74
Preprint. Discussion started: 29 March 2021

3.3. Element composition of point measurements (EPMA)

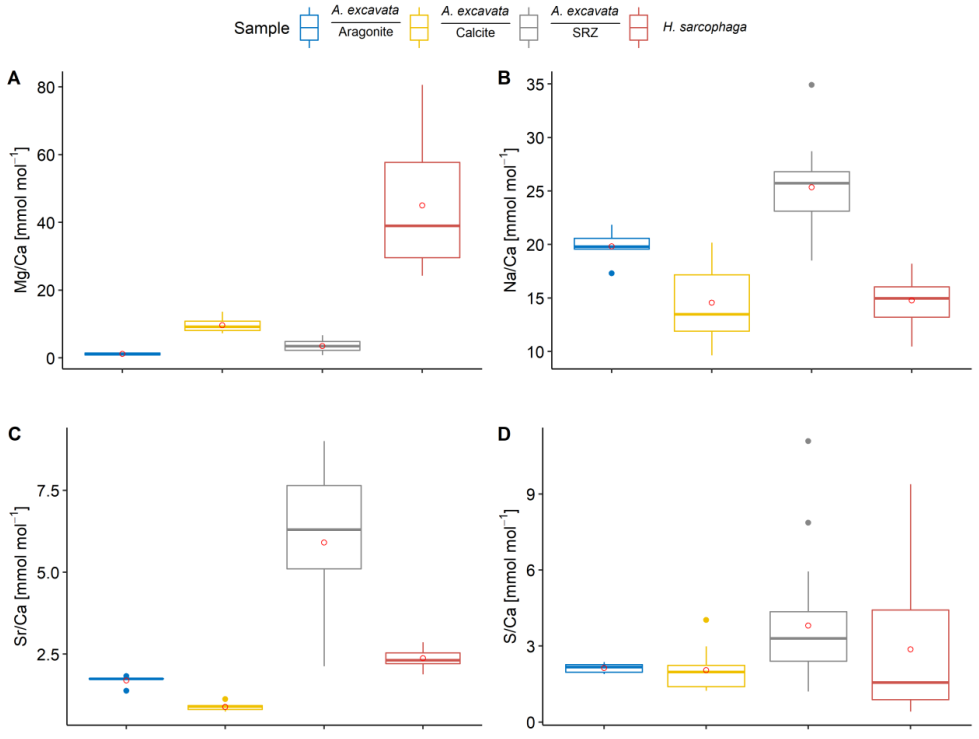

Figure 2 Results of point measurements by EPMA in different sections of *A. excavata* and *H. sarcophaga* (two specimen each). A: Mg/Ca, B: Na/Ca, C: Sr/Ca, D: S/Ca. Red circles show the mean values.

Within the bivalve shell Mg/Ca varies between 0.76 and 13.6 mmol mol^{-1} (Fig. 2). Lowest values were found in the aragonitic shell layer (Fig 1/E_3) and highest values are measured in the calcitic shell layers (Fig 1/$E_{1\&2}$). With a mean ratio of 3.47 mmol mol^{-1}, the SRZ is enriched in Mg/Ca compared to the undisturbed bivalve aragonite. The highest Mg/Ca ratios are measured in the foraminiferal calcite (mean = 45.03 mmol mol^{-1}, max = 80.6 mmol mol^{-1}).

Na/Ca ratio show similar values in the different sections when considering the carbonate polymorph, they are built of. The aragonitic sections (Fig 1/E_3), bivalve aragonite and SRZ, have mean Na/Ca ratios of 22.0 and 25.3 mmol mol^{-1} respectively. The SRZ displays a higher variability than the undisturbed aragonite. Both calcitic regions are characterised by mean Na/Ca of 14.8 mmol mol^{-1} (Fig 1/$E_{1\&2}$).

https://doi.org/10.5194/bg-2021-74
Preprint. Discussion started: 29 March 2021


Biogeosciences
Discussions
Open Access
EGU

232 The SRZ is enriched in Sr/Ca compared to the undisturbed shell sections. Mean ratios are with 5.91
233 mmol mol^{-1}nearly four times higher than in the undisturbed aragonitic shell parts (mean = 1.54 mmol
234 mol^{-1}. Lowest values are measured in the bivalve calcite (mean = 0.89 mmol mol^{-1}).

235 S/Ca ratios are comparable in the undisturbed bivalve aragonite and calcite, with 1.9 and 2.1 mmol
236 mol^{-1}, respectively. Similar to Sr/Ca, the highest mean and maximum S/Ca ratios are measured in the
237 SRZ (mean = 3.8 mmol mol^{-1}, max = 11.1 mmol mol^{-1}).

238 The Ca concentration in the different samples varies between 36.7 w% and 39.3 w%. Variations in E/Ca
239 ratios are therefore not necessarily controlled by changes of the observed element but can also change
240 according to the Ca concentration. However, changes in the Ca concentration are negligible in the
241 context of this study as the maximum deviation of the calculated E/Ca ratios amounts to 2 mmol mol^{-1}
242 for Mg/Ca at 80 mmol mol^{-1}

https://doi.org/10.5194/bg-2021-74
Preprint. Discussion started: 29 March 2021

3.4. EPMA element maps

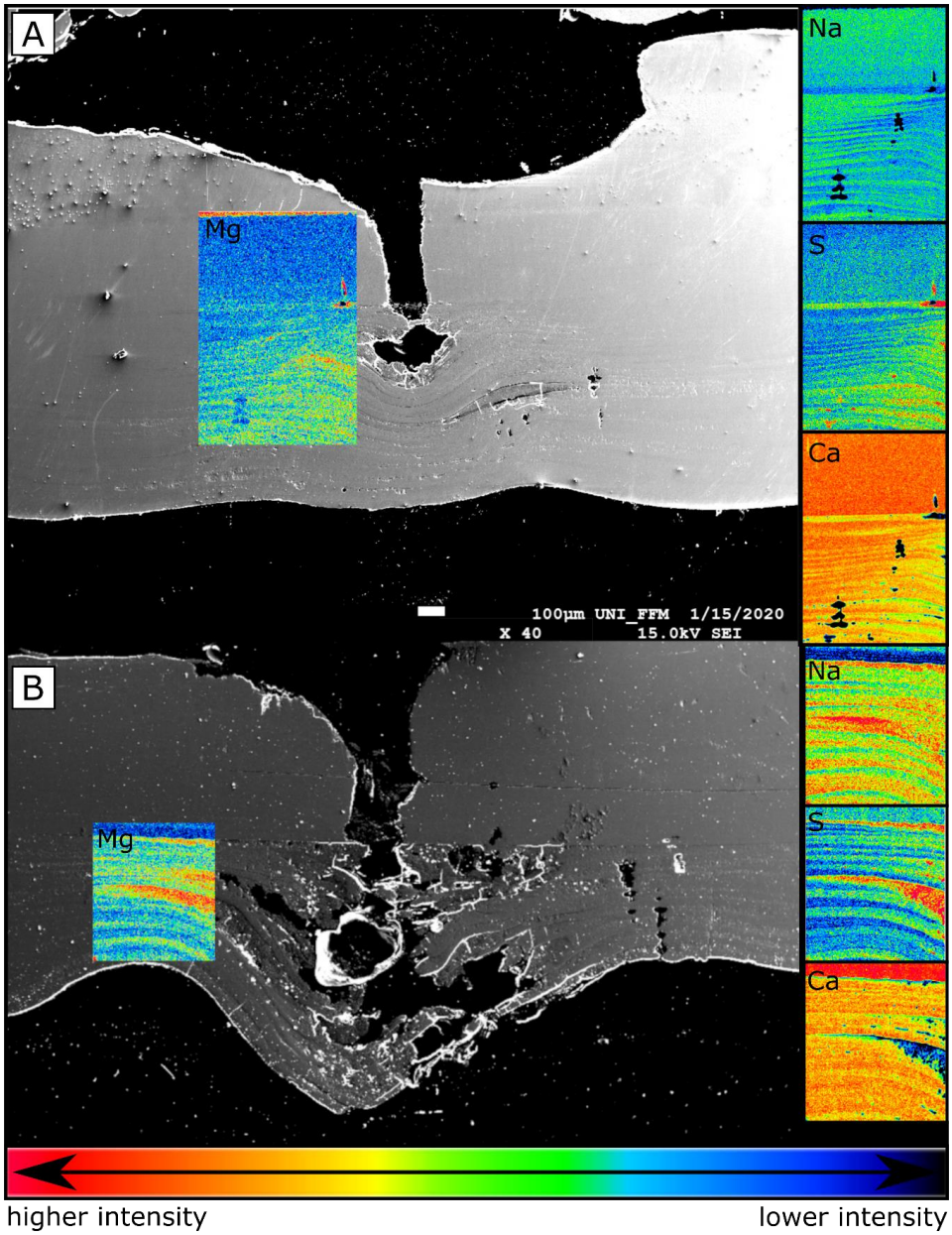

Figure 3 EPMA element maps and secondary-electron image from an SEM of the callus area of *A. excavata*.

As was visible in the fluorescence image (Fig. 1), the EPMA chemical maps show a similar layering pattern (Fig. 3). Areas rich in magnesium also show increased sodium and sulfur intensities whereas calcium intensities are lower.

https://doi.org/10.5194/bg-2021-74
Preprint. Discussion started: 29 March 2021

Biogeosciences
Discussions
Open Access
EGU

3.5. Stable carbon and oxygen isotope

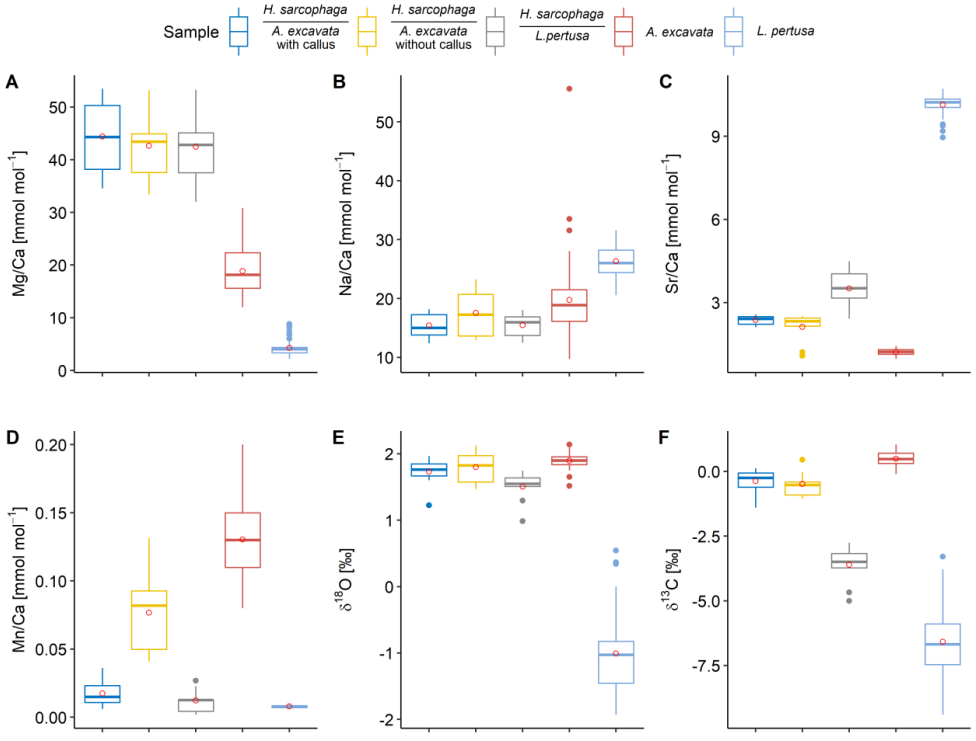

Figure 4 Box- and whisker plots displaying the E/Ca (ICP-OES and ICP-MS) and stable isotope measurements (MS) of the investigated specimens. Red circles show mean values.

The different *H. sarcophaga* shells exhibit differences in their isotopic composition based on their host organism (Fig. 4 E/F). In particular, $\delta^{18}O$ values are similar in HL and HA with +1.64 ‰ and +1.80 ‰, respectively. These values are in accordance with $\delta^{18}O$ values from the host organism *A. excavata*, which range from +1.52 ‰ to +2.2 ‰. L. pertusa displays lower $\delta^{18}O$ and $\delta^{1C}C$ values, ranging from -1.93 ‰ to +0.54 ‰ and -9.40 ‰ to -3.29‰.

Bigger differences between *H. sarcophaga* samples, are observable in the carbon isotopic signature of specimens taken from different host organisms. HA display $\delta^{13}C$ values of -0.43 ‰ which is close to the ratios of their host organism, being +0.5 ‰. HL are more depleted in heavy carbon isotopes with a measured value of -3.97 ‰. For reference, the isotopic composition of the ambient seawater is $\delta^{18}O$ = +0.26 ‰ and $\delta^{13}C$ = +0.38 ‰.

The isotopic composition of HAW and HAO can be described by linear functions whereas the isotopic composition in HL cannot:

https://doi.org/10.5194/bg-2021-74
Preprint. Discussion started: 29 March 2021

$\delta^{13}C_{HAW} = 1.8\pm0.4*\delta^{18}O\text{-}3.4\pm0.8$ ($r^2 = 0.7$, p=0.004, df = 7) [1]

$\delta^{13}C_{HAO} = 1.1\pm0.3*\delta^{18}O\text{-}2.6\pm0.6$ ($r^2 = 0.6$, p=0.02, df = 6) [2]

$\delta^{13}C_{HL} = 1.7\pm1.0*\delta^{18}O\text{-}6.2\pm1.5$ ($r^2 = 0.18$, p=0.12, df = 8) [3]

3.6. ICP-OES results from *H. sarcophaga* grown on different host organisms

H. sarcophaga samples from different host organisms are similar in their chemical composition with regard to Mg/Ca and Na/Ca (Fig. 4 A/B). Mean Mg/Ca ratios range from 42.4 to 44.4 mmol mol^{-1}, with intra-individual variations of 6.8 – 7.2 mmol mol^{-1} (SD). Both host organisms have lower mean Mg/Ca ratios of 4.2 mmol mol^{-1}and 18.9 mmol mol^{-1} in *L. pertusa* and *A. excavata*, respectively.

Mean Na/Ca ratios range between 15.5 – 16.2 mmol mol^{-1} for *H. sarcophaga*. The highest Na/Ca ratios and variations are measured in HAO. *L. pertusa* displays overall higher Na/Ca ratios than *H. sarcophaga* (25.6 mmol mol^{-1}). The highest variation is measured in *A. excavata* ranging from 9.8 – 55.6 mmol mol^{-1}with a mean of 19.8 mmol mol^{-1}.

A clear difference in Sr/Ca of 1.1 ± 0.16 (2SD of MACS3) mmol mol^{-1} is evident between *H. sarcophaga* from the different host organisms (Fig. 4 C). HAW and HAO show mean Sr/Ca ratios of 2.37 and 2.36 mmol mol^{-1}, respectively. The host organism *A. excavata* has lower Sr/Ca ratios (1.2 mmol mol^{-1}). On the contrary, HL and *L. pertusa*, display higher mean Sr/Ca ratios of 3.5 and 10.2 mmol mol^{-1} respectively.

Prominent differences between *H. sarcophaga* groups are also evident in their Mn/Ca ratios (Fig. 4 D). HAW, HL and *L. pertusa* display Mn/Ca ratios of 0.010 – 0.017 mmol mol^{-1} whereas HAO and *A. excavata* show higher Mn/Ca ratios of 0.066 and 0.13 mmol mol^{-1}, respectively.

3.7. Compositional differences in *H. sarcophaga* related to their host organism

Table 1 Results of the one-way ANOVA and Kruskal-Wallis analysis with the host organism as predictor variable. Bold fields show elemental and isotopic ratios in *H. sarcophaga* that may be significantly influenced by the chemistry of the host organism.

	Mg/Ca	Na/Ca	Sr/Ca	Mn/Ca	$\delta^{18}O$	$\delta^{13}C$
ANOVA						
DFn	2					
DFd	25					
F	0.2	0.22	23	32	4.1	97
p	0.82	0.8	**<0.001**	**<0.001**	**0.029**	**<0.001**
Generalized eta squared	0.015	0.018	0.65	0.74	0.26	0.89
Kruskal-Wallis test						
n	28					
df	2					
p	0.83	0.92	**<0.001**	**<0.001**	**0.03**	**<0.001**

https://doi.org/10.5194/bg-2021-74
Preprint. Discussion started: 29 March 2021

We conducted a one-way ANOVA and Kruskal Wallis test (Table 1) in order to explore if the investigated *H. sarcophaga* groups (HAW, HAO, HL) show significant differences in their geochemical composition related to their host organism. We used the measured elemental- and isotopic composition as target variable and the host organisms (*A. excavata* with callus, *A. excavata* without callus, *L. pertusa*) as factor variable. Tukey-HSD (Table 2) was used as post-hoc test to investigate group specific mean differences.

Table 2 Tukey-HSD test results. Bold fields show significant differences between the two groups.

Tukey-HSD test				
	Group 1	**Group 2**	**Difference**	***p***
Mg/Ca	HAW	HAO	-1.22	0.93
	HAW	HL	-1.95	0.81
	HAO	HL	-0.73	0.97
Na/Ca	HAW	HAO	0.74	0.81
	HAW	HL	0.05	0.99
	HAO	HL	-0.68	0.84
Sr/Ca	HAW	HAO	-0.004	1
	HAW	HL	1.14	**<0.001**
	HAO	HL	1.14	**<0.001**
Mn/Ca	**HAW**	HAO	0.05	**<0.001**
	HAW	HL	-0.005	0.75
	HAO	HL	-0.05	**<0.001**
$\delta^{18}O$	HAW	HAO	0.07	0.81
	HAW	HL	-0.23	0.11
	HAO	HL	-0.30	**0.032**
$\delta^{13}C$	HAW	HAO	-0.11	0.91
	HAW	HL	-3.24	**<0.001**
	HAO	HL	-3.12	**<0.001**

The one-way ANOVA reveals no significant in the Mg/Ca and Na/Ca ratios of the foraminifera that were collected from the different host organisms (Table 1). In contrast, the ANOVA suggests a significant difference between Sr/Ca and Mn/Ca ratios between these two groups. In the case of Sr/Ca, significant differences based on the Tukey-HSD post-hoc test are observable between HL and HA, whereas we find no significant differences between HAW and HAO. In addition, we observe no significant differences between HAW and HL in their Mn/Ca composition, but significant differences are present between both these groups and HAO.

In the case of the stable oxygen isotope composition, we observe significant differences between *H. sarcophaga* specimens from different host organisms. The $\delta^{18}O$ ratio measured in HL is significantly lower than in HAO. Significant differences are also observable for $\delta^{13}C$ ratios. Here, differences in the isotopic composition are detectable between HL and HA, with the latter showing higher $\delta^{13}C$ ratio.

https://doi.org/10.5194/bg-2021-74
Preprint. Discussion started: 29 March 2021

309 The Kruskal-Wallis test, which was used as a non-parametric cross validation for the ANOVA test, shows
310 the same results as the ANOVA test

311 4. Discussion

312 4.1. Sr/Ca differences in *H. sarcophaga* related to the host organism

313 We observe significant differences in the Sr/Ca and Mn/Ca composition between *H. sarcophaga* from
314 different host organisms.

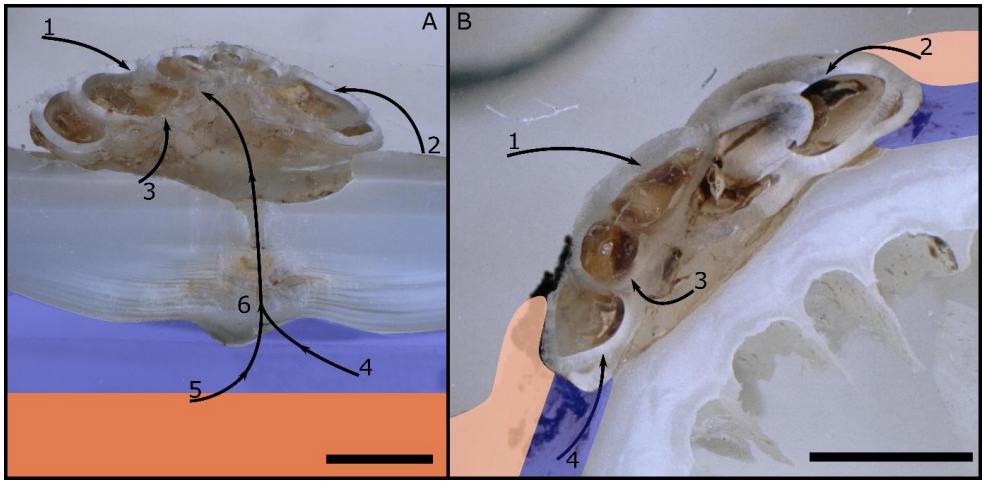

315

316 Figure 5 Possible pathways of E/Ca and isotopic signals into the foraminiferal calcite.
317 A: *H. sarcophaga* on *A. excavata*, B: *H. sarcophaga* on *L. pertusa*. Blue areas represent the calcifying space, orange areas
318 represent mantle tissue in *A. excavata* (A) and organic layer (coenosarc/mucus) in *L. pertusa* (B). Uptake of seawater and
319 free-floating particles (1), Ingestion of host organic material (periostracum, coral tissue/mucus) (2), Ingestion of dissolved
320 carbonate material (3), Ingestion of extracellular calcifying fluid (ECF) (4), Ingestion of Mantle tissue (5), ingestion of
321 carbonate and organic material from the deposited callus (6). Scalebar is 100 µm. Please note that the calcifying space and
322 organic layers are displayed enlarged for improved visibility. Actual size of the calcifying space amounts to 1-100 nm
323 (Nakahara, 1991; Tambutté et al., 2007). The organic layer (coenosarc) is ~ 25 µm in thickness (Tambutté et al., 2007).

324 HL show significantly higher Sr/Ca ratios than HA. Given that this result is based on measurements
325 from multiple individuals distributed across more than one host organism, we suggest that this is most
326 likely a signal of the high Sr/Ca aragonite precipitated from *L. pertusa* that is imprinted into the test of
327 *H. sarcophaga*. In both host organisms, *H. sarcophaga* produces an attachment etching on the host
328 (Fig. 3) to firmly anchor itself (Bromley and Heinberg, 2006). It subsequently penetrates the host shell
329 in order with their pseudopodia to access the hosts soft tissue (Beuck et al., 2008). The attachment
330 etching may additionally serve to satisfy the calcium-requirements of *H. sarcophaga* for the
331 calcification of its shell (Cedhagen, 1994), rather than expending further energy to source Ca from the
332 surrounding seawater. By chemically corroding the attachment etching as well as by the penetrating
333 boring and by taking up the resulting solutions, the foraminifer gains access to a pre-concentrated
334 calcium carbonate solution from which it can precipitate its shell (Fig. 5). Naturally, the foraminifer

https://doi.org/10.5194/bg-2021-74
Preprint. Discussion started: 29 March 2021

would also reflect other characteristics of the host, such as the high Sr/Ca ratio from the aragonite of *L. pertusa* (Raddatz et al., 2013; Schleinkofer et al., 2019). In agreement with the much lower Sr/Ca ratios in calcite and aragonite in *A. excavata* (Schleinkofer et al., 2021) compared to the coralline aragonite, we do not observe such high Sr/Ca ratios in HA. Still, the observed Sr/Ca ratios in HA are higher by a factor of two than in the host organism. Since we do not observe differences between HAW and HAO, the Sr/Ca surplus cannot be derived from the ingestion of organic material from within the shell cavity. A further control is likely provided through the mixture of dissolved host $CaCO_3$ material and ambient seawater from which the foraminifer calcifies, which is explored further in the next section.

4.2. Mixing model

In order to further investigate underlying mechanisms of the observed results we created a simple two-component model to explore how the trace-element chemistry of *H. sarcophaga* could change by delivery of ions to the calcification site that were derived from dissolution of the host organism. In this model we calculate changes of the foraminifera composition in dependence from an assumed calcification from a variable mixture of seawater and dissolved host carbonate material. We excluded the addition of the hosts calcifying fluid in the model because there is no data available for the chemical composition of the calcifying fluid of *L. pertusa* nor *A. excavata*, and because the model is intended only as an initial exploration of whether the geochemistry of *H. sarcophaga* can be explained in this way. Furthermore, measurements of the chemical composition of the calcifying fluid of other bivalve species indicate that the composition is close to the composition of seawater (Crenshaw, 1972; Wada and Fujinuki, 1974).

The model calculates element/Ca ratios based on calcite precipitation from a fluid that is derived from a mix of seawater (transported to the calcification site, see e.g. (Erez, 2003)), and $CaCO_3$ dissolved from the host organism:

$$\frac{E}{Ca_{Hyrrokin}} = \frac{E_{SW} + \frac{10^R}{M_{Carb}} * \frac{\frac{E}{Ca_{Host}}}{1000}}{Ca_{SW} + \frac{10^R}{M_{Carb}}} * D_E \quad [4]$$

E_{SW} = element concentration in seawater, E/Ca_{Host} = element/Ca in host carbonate [mmol mol^{-1}], Ca_{SW} = Calcium concentration in seawater (10 mmol L^{-1}), D_E = Calcite-Water distribution coefficient, M_{Carb} = atomic mass of $CaCO_3$ (100.08 g mol^{-1}) and R = log mixing ratio between carbonate and seawater [g/L].

Table 3 Parameters used in the proposed model to explore the effects of carbonate and water uptake of *H. sarcophaga* on the shell chemistry. Host element/Ca ratios are derived from this study.

Model parameters			
E_{SW} [mmol L^{-1}]	E/Ca_{Acesta}	$E/Ca_{Lophelia}$	D_E

https://doi.org/10.5194/bg-2021-74
Preprint. Discussion started: 29 March 2021

		[mmol mol^{-1}]	[mmol mol^{-1}]	
Mg/Ca	53	19	4.2	0.015 (Segev and Erez, 2006)
Na/Ca	450	20	26	0.0016 (Allen et al., 2016)
Sr/Ca	0.1	1.2	10.1	0.28 (Raitzsch et al., 2010)
Mn/Ca	5*10^{-6}	0.131	0.008	13 (Mucci, 1988)

As we have no information about the amount of dissolved material and water that is taken up by H. sarcophaga, we modelled it over eight orders of magnitude (log dissolved $CaCO_3$/seawater ratios of -4 to +4). This corresponds to a range from 99.99 % seawater and 0.01 % host $CaCO_3$ contribution to 0.01 % seawater and 99.99 % host $CaCO_3$ contribution. The parameters used are reported in Table 3.

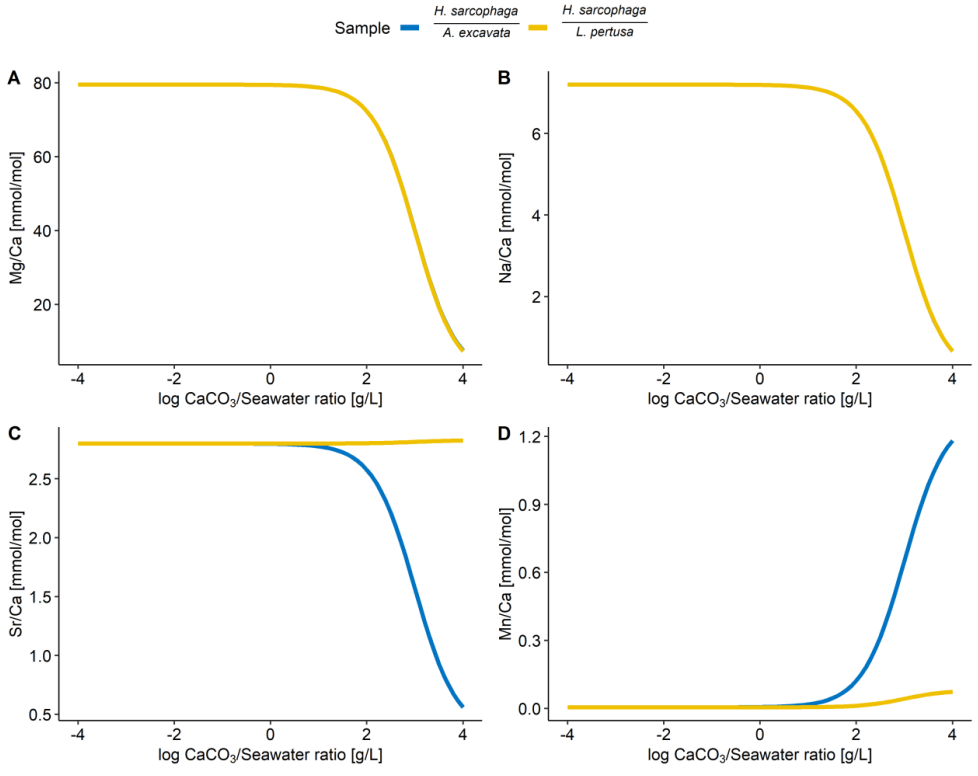

Figure 6 Results of model calculations with the aforementioned parameters for the measured E/Ca ratios. Independently of the mixing ratio of dissolved host $CaCO_3$ and ambient water, no differences of the geochemical signature is predictable in Mg/Ca and Na/Ca. On the contrary, Sr/Ca and Mn/Ca ratios are predicted to diverge at mixing ratios > 10 g $CaCO_3$/ L seawater

Based on the proposed model, we can see that the Mg/Ca and Na/Ca ratios in *H. sarcophaga* are independent of the geochemical signature of the host it lived on. This is caused by the high concentration of these elements in the ambient seawater in comparison to the host's carbonate. The

https://doi.org/10.5194/bg-2021-74
Preprint. Discussion started: 29 March 2021

composition of the mixture is largely controlled by the addition of Ca, which is equal for both host organisms.

In contrast, the model predicts that, at high ratios of $CaCO_3$ derived from the host compared to the surrounding seawater, different Sr/Ca and Mn/Ca ratios should be observed between foraminifera living on different host organisms. The modelled Sr/Ca ratios for HL are constant at 2.8 mmol mol^{-1} independent from the mixing ratio (Fig. 6C). This is because when the foraminifera dissolves aragonitic material of *L. pertusa* and mixes it with seawater, the resulting Sr/Ca ratios in this solution do not change due to the aragonitic D_{Sr} being close to 1. Consequently, if the shell Sr/Ca ratio in *H. sarcophaga* depends on calcite D_{Sr} and the Sr/Ca ratio in the calcifying fluid of *H. sarcophaga*, the resulting Sr/Ca ratio in HL is equivalent to a specimen that calcifies solely from seawater (specimen without a host). As the calcitic D_{Sr} is below 1 (Mucci and Morse, 1983; Raitzsch et al., 2010), the addition of dissolved material from *A. excavata* in the calcifying space results in decreasing Sr/Ca ratios in the calcifying fluid and consequently lower Sr/Ca ratios in the precipitated calcite of the foraminifera. Similar results are obtained in the case of Mn/Ca ratios. The addition of dissolved host material to the calcifying space of *H. sarcophaga* results in an increase of the Mn/Ca ratio in the calcifying fluid, which leads to increasing Mn/Ca ratios in the foraminiferal calcite.

While the proposed model can explain why we do not see changes in the Mg/Ca and Na/Ca composition of H. sarcophaga from different host organisms, and can also explain why Sr/Ca ratios differ between these groups (Fig. 2) it cannot explain the occurring processes entirely. The model can only predict Na/Ca ratios up to 7 mmol mol^{-1} (Fig. 6B), whereas we measure ratios of 15 mmol mol^{-1}. As already mentioned, this is a simplified model that disregards possible influences of other reservoirs such as the calcifying fluid of the bivalve that might also form part of the calcifying fluid of H. sarcophaga. Additionally, the distribution coefficients used in this model are not empirically determined on *H. sarcophaga* but derive from other benthic foraminifera (Mg/Ca, Na/Ca, Sr/Ca) or inorganic precipitation experiments (Mn/Ca) , and the model also does not account for growth-rate driven differences in trace element portioning, which are especially relevant in the case of Na and Mn (Füger et al., 2019; Mucci, 1988).

4.3. Mn/Ca differences in *H. sarcophaga* related to the host organism

Based on the ANOVA analysis (Table 1), significant differences are also observable in the Mn/Ca ratios. HAO display four times higher Mn/Ca ratios then in the other two observed groups. HL show similar Mn/Ca ratios as their host organism, both HAW and HAO show lower Mn/Ca ratios. Based on the differences, we observe between the samples that were picked from *A. excavata*, it is unlikely that the Mn/Ca signal in *H. sarcophaga* derives from the host shell material (Fig. 5/A3 & B3). In this case we

https://doi.org/10.5194/bg-2021-74
Preprint. Discussion started: 29 March 2021

411 would expect to see differences between HA and HL as Mn/Ca in *A. excavata* is approximately one
412 order of magnitude higher than in *L. pertusa*. Influences of the surrounding water cannot explain the
413 observed differences either. Manganese, as a redox-sensitive element, is controlled by the oxygen
414 concentration of the ambient water. Under well oxygenated conditions, the main species Mn^{2+} is
415 oxidized to Mn-oxyhydroxides and precipitated (Calvert and Pedersen, 1993, 1996). Low-oxygen
416 conditions lead to a reduction of Mn-oxyhydroxides to the bioavailable Mn^{2+} and an consequent
417 increase of Mn/Ca ratios in biogenic carbonates (Groeneveld and Filipsson, 2013; Koho et al., 2015;
418 Tribovillard et al., 2006). However, the Leksa Reef is well oxygenated (Jacobson, 1983; Milzer et al.,
419 2013).

420 An influence of the calcification rate on Mn/Ca ratio was shown in inorganic precipitated calcite
421 overgrowths and the planktic foraminifer *Orbulina universa* (Holland et al., 2017; Lorens, 1981; Mucci,
422 1988). Generally speaking, increased calcification rates cause Mn/Ca ratios in the precipitates to
423 decrease (Holland et al., 2017; Mucci, 1988). In our investigated samples, this effect would imply lower
424 calcification rates in HAO compared to HAW and HL. The possibility of HAO having low calcification
425 rates is likely, as it is missing its primary nutrient source. Due to the high distribution coefficient of
426 manganese, Rayleigh fractionation, might add an additional control on Mn/Ca ratios in the
427 foraminifera shell (Holland et al., 2017). The model of Rayleigh fractionation relies on a number of
428 assumptions about the internal reservoir of the foraminifera concerning size, initial composition,
429 refreshment rate and calcification rate (Elderfield, 1996). As these parameters are not fully understood
430 we cannot provide further information about the possible influence.

431 A significant influence of possibly Mn-enriched bodily fluids of bivalves (Wada and Fujinuki, 1974) can
432 also not explain the differences in the chemical composition as the samples that discern from the
433 others are picked from HAO. These foraminifera did not have access to the internal organic material
434 of the bivalve (Fig. 5/A4). Instead, the high Mn signal in HAO must derive from a source that is located
435 on the outside of the bivalve host (Fig. 5/A2). When the foraminifera initially infests the bivalve and
436 starts boring into the shell, nutrient sources other than the internal organic parts of the bivalve have
437 to be utilised by *H. sarcophaga.* The organic periostracum of the bivalve could depict this nutrient
438 source as it is a highly nutritional source for organic material on the outside of the bivalves shell (Secor
439 et al., 1993). High concentrations of Mn and Fe were measured in the periostracum of freshwater and
440 marine bivalves (Allen, 1960; Swinehart and Smith, 1979). The mechanistic explanation for this
441 enrichment of Mn and Fe is reported to be the high amount of the amino acids containing glycine and
442 tyrosin in the periostracum of bivalves (Hare, 1965; Whitney et al., 2019), which act as complexing
443 sites for metal ions (Swinehart and Smith, 1979). The existence of living *H. sarcophaga* attached to
444 rocks demonstrates that they do not necessarily rely on a living host but can also supply themselves

https://doi.org/10.5194/bg-2021-74
Preprint. Discussion started: 29 March 2021

through other feeding strategies (Cedhagen, 1994). Since algae take up Mn and concentrate it internally (Sunda and Huntsman, 1985), the increased Mn/Ca in HAO could also be caused by an facultative suspension feeding mode of *H. sarcophaga* during its early ontogeny.

At this point we can only speculate about the mechanistic explanation for the enrichment of Mn/Ca in HAO. Future research on *H. sarcophaga* should involve spatially resolved Mn and Fe measurements, to explore if there is an ontogenetic decrease of Mn/Ca ratios in the test of *H. sarcophaga* picked from *A. excavata*. This decrease would mark the time of the first penetration of the bivalve shell.

4.4. Carbonate isotopic composition in *H. sarcophaga* based on the host organism

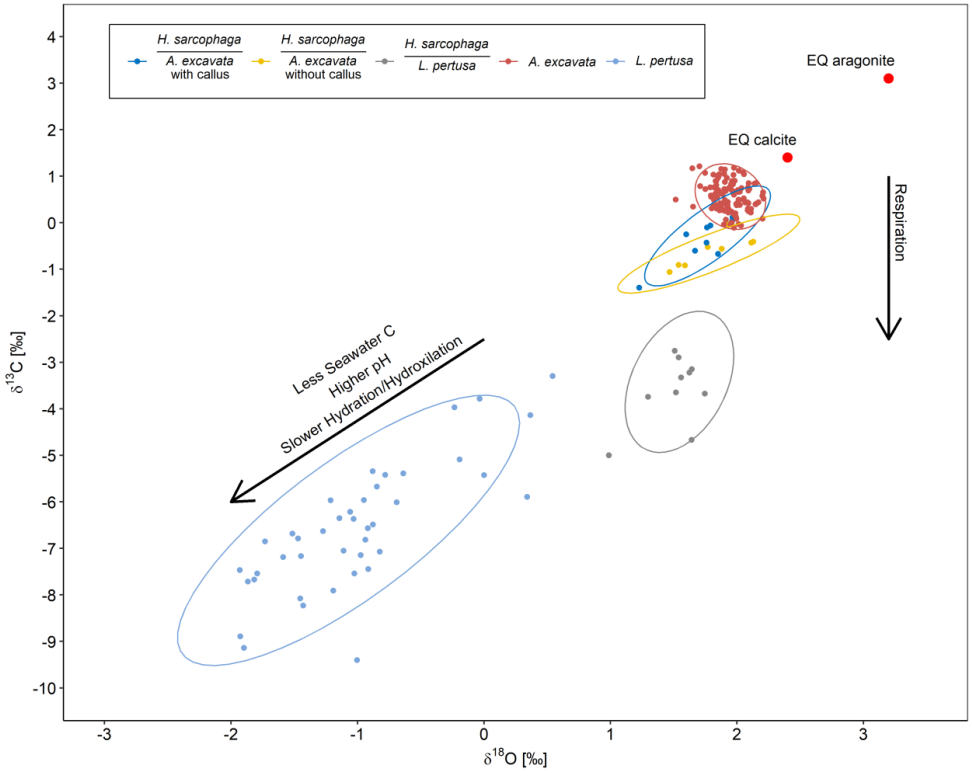

Figure 7 $\delta^{18}O$ plotted against $\delta^{13}C$ for *H. sarcophaga* from different host organisms and for the host organisms with 95 % confidence ellipse. Arrows show compositional changes induced by kinetic effects and respiration. Text in the denominator is the host organism that *H. sarcophaga* grew on. Red points show the equilibrium composition for calcite and aragonite as calculated from the isotopic composition of the ambient seawater.

The oxygen and carbon isotopic composition of the different organisms are characterised by large differences. *A. excavata* does not show signs of kinetic effects which would be indicated by a correlation of $\delta^{13}C$ and $\delta^{18}O$ values (Adkins et al., 2003; Bajnai et al., 2018; McConnaughey, 2003). Bivalves are largely considered to calcify in equilibrium with the surrounding water (Immenhauser et

https://doi.org/10.5194/bg-2021-74
Preprint. Discussion started: 29 March 2021

al., 2016), which appears to be valid for *A. excavata* as it displays an isotopic composition close to the expected equilibrium (Fig. 7). The host organism *L. pertusa* displays higher departures from the expected aragonite equilibrium, which is mainly caused by additional incorporation of isotopically lighter, metabolic CO_2 and by kinetic isotope effects associated with hydration/hydroxylation reactions given that this coral raises the calcification site pH to values significantly exceeding seawater pH (Adkins et al., 2003; Chen et al., 2018; Holcomb et al., 2009).

Interestingly, the *HA* samples display an isotopic composition very similar to the composition of its host organism (Fig. 7). The 95% confidence ellipsoids of HAW, HAO and *A. excavata* all overlap at highest $\delta^{18}O$ values. However, in contrast to *A. excavata,* HAW and HAO display positive correlations between $\delta^{18}O$ and $\delta^{13}C$. This may indicate that all three organisms closely mineralize their carbon from the same source, but hydration/hydroxylation kinetics occur more pronounced in HAW and HAO relative to *A. excavata.*

The observable differences in the carbon isotopic composition between HA and HL can also be caused by different proportions of the carbon sources. HL presumably have constant access to the host's carbon pool, whereas the access of HA to the host's carbon pool is limited due to the defence mechanism of *A. excavata* (Fig. 3). When the bivalve has successfully closed the boring of the foraminifer, the foraminifer must use seawater DIC as a carbon source until it penetrated the shell again. This mixing of different carbon sources in HA in contrast to the stable carbon source of HL can explain the lower $\delta^{13}C$ values in HL due to an increased influence of host derived carbon.

HL is characterized by significantly more positive $\delta^{18}O$ values than its host, and it also shows a slightly steeper positive correlation between $\delta^{13}C$ and $\delta^{18}O$. Both circumstances point to faster hydration/hydroxylation kinetics to be effective during the mineralization of HL compared to its host (Chen et al., 2018). If the pH at which HA precipitates its carbonate is lower than the pH of the calcifying fluid in *L. pertusa*, the hydration kinetics would be accelerated as a result(Cohen, 2003; Crenshaw, 1972; Raddatz et al., 2014). Both organisms may derive their carbon from the same source which likely occurs depleted in ^{13}C relative to seawater, possibly due to significant admixture from metabolic CO_2. This assertion is supported by the fact that HL has constant access to the host's carbon pool.

4.5. Implications for paleoceanographic reconstructions

The results presented here have implications for paleoreconstructions in two ways. When using bivalves for paleo reconstructions or geochemical investigations in general, the shells must be carefully examined for potential traces of bioerosion. In case of callus formation, the carbonate formed can have a significantly different composition than the original carbonate mineralogy.

https://doi.org/10.5194/bg-2021-74
Preprint. Discussion started: 29 March 2021

494 Even more critical are the implications for paleoreconstructions using foraminifera which are regularly
495 analyzed for this purpose. Several foraminifera species are known to live on different host organisms
496 and act as parasites and/or bioeroders (Dupuy et al., 2010; Freiwald and Schönfeld, 1996; Walker et
497 al., 2017). Some of these are also used for isotope and element based paleoenvironmental
498 reconstructions or geochemical investigations in general, such as *Cibicides refulgens* (García-Gallardo
499 et al., 2017; Mackensen and Nam, 2014; Rathburn and De Deckker, 1997), *Hanzawaia concentrica*
500 (Smith and Emiliani, 1968) and *Discanomalia coronata* (Baranwal et al., 2014).

501 As an example we use a $\delta^{18}O$-temperature conversion formula for benthic foraminifera (Marchitto et
502 al., 2014) and our measured $\delta^{18}O$ ratios to reconstruct a temperature for the Leksa Reef of 7.5 °C using
503 HAO and 7.8 °C using HAW. *In-situ* measurements of the water temperature in the Leksa Reef by CTD
504 show a mean temperature of 7.8°C (min= 7.1°C, max=8.8°C) (Büscher, 2018). If we however use $\delta^{18}O$
505 ratios from HL we would reconstruct a water temperature of 8.8°C and consequently overestimate the
506 water temperature by 1.0 °C

507 If the aforementioned species show similar host specific alterations of their isotopic and elemental
508 composition, paleotemperature reconstructions on the basis of these species could be biased. Given
509 that our results indicate that host specific isotopic and elemental composition changes can be present
510 in the parasitic foraminifer *H. sarcophaga* we draw attention to other parasitic foraminifera that should
511 be investigated for similar host-parasite relations, especially if they are used for geochemical
512 investigations.

513 **4.6. Biomineralization in the callus region**

514 In order to protect itself from the parasitizing foraminifer, *A. excavata* seals the canal etched through
515 the shell. This is accomplished by rapidly calcifying over the foraminifera boring (Beuck et al., 2008;
516 Cedhagen, 1994). The calcification process produces a callus on the inside of the bivalve shell that is 3-
517 5 mm in diameter and 1-2 mm in height. In the SRZ we can observe the proposed model of
518 biomineralization in bivalves that starts with the formation of an organic sheet, indicated by the high
519 fluorescence, high S concentration and low Ca- concentration, which acts as a framework during
520 calcification (Addadi et al., 2006; Checa et al., 2005; Wada, 1976). The following layer is depleted in S
521 and enriched in Ca and therefore represents a higher $CaCO_3$ concentration (Fig. 1 & 3). This sequence
522 is repeated multiple times leading to the formation of the visible callus. As long as the foraminifera
523 does not stop the boring process, the bivalve needs to continually counter calcify the region of
524 infestation to defend itself.

525 The callus displays high concentrations of organic material, that is not observable in the undisturbed
526 regions. The layers that are characterised by high organic contents appear to be preferentially

https://doi.org/10.5194/bg-2021-74
Preprint. Discussion started: 29 March 2021

dissolved (Fig. 3B) In cross sections, organic rich areas make up 50 % of the callus (Fig 1/D). It appears unlikely that the high amounts of organic material in the SRZ are solely deposited as a calcification framework, considering the differences between undisturbed shell areas and the SRZ. Therefore, the high amount of deposited organic material probably serves some other purpose, such as an increase of the overall material deposition rate and the provision of an initial sealant from the surrounding water.

The boring organisms pose a threat to the bivalve in multiple ways. It has been shown that *H. sarcophaga* penetrated the mantle of *A. excavata* which led to a destruction of the mantle epithelium of the bivalve due to ingestion by *H. sarcophaga* (Cedhagen, 1994). Infested sections showed larger numbers of cell nuclei, indicating higher cell division rates and higher metabolic rates (Cedhagen, 1994). The pathway through the bivalve shell furthermore allows pathogens to reach and attack the bivalve and allows surrounding water to permeate into the extra pallial fluid (EPF) of the bivalve. Even though the EPF in several bivalve species shows trace element concentrations close to seawater (Crenshaw, 1972; Wada and Fujinuki, 1974), the bivalve still has to actively concentrate Ca in the calcifying space to reach concentrations that exceed the solubility product (Bonucci and Wheeler, 2020; Wilbur and Saleuddin, 1983). This concentration of Ca is accomplished through active pumping by means of enzymes such as Ca-ATPase (Klein et al., 1996) or through ion channels (Carré et al., 2006). In case of an unsealed calcifying space, the dilution with seawater makes high concentrations of Ca-ions to levels needed for calcification in the extra EPF less likely. A fast-sealing method, by means of organic deposition, is therefore necessary to ensure that the bivalve's calcification capability is not compromised.

Geochemically, the SRZ shows the largest differences to the undisturbed aragonite in Mg/Ca and Sr/Ca ratios (Fig 2 & 3). Mg/Ca ratios are five times higher in the SRZ than in undisturbed aragonite. Magnesium is regarded to be enriched in organic matrices secreted by the bivalve compared to the shell $CaCO_3$ (Schöne et al., 2010). The distribution of magnesium in the SRZ, especially its enrichments in fluorescent layers rich in sulfur (Fig. 1 & 3), makes an enrichment of Mg due to high organic concentrations likely. Beside an enrichment of Mg in the secreted organic matter, peptides similar to that found in sites of calcification (Moradian-Oldak et al., 1990) can increase the Mg concentration in precipitated calcite by reducing the dehydration enthalpy (Stephenson et al., 2008). These peptides are also regularly found in molluscs (Falini et al., 1996; Halloran and Donachy, 1995; Marin et al., 2007; Zhang and Zhang, 2006). As these peptides do furthermore increase the growth rate by 25 % to 50 % (Stephenson et al., 2008), due to the need of fast calcification (Beuck et al., 2008), a high concentration of the peptides in SRZ is supported. Higher growth rates can furthermore lead to an increase of crystal impurities which could alter other elements besides Mg (Lorens, 1981).

https://doi.org/10.5194/bg-2021-74
Preprint. Discussion started: 29 March 2021

In contrast to magnesium, strontium was not found to be enriched in organic matter compared to shell $CaCO_3$ (Takesue et al., 2008). However, the influence of peptides on other elements such as Sr is speculated on (Stephenson et al., 2008). Sr in aragonitic bivalves is considered to be controlled by growth rate effects (Carré et al., 2006; Füllenbach et al., 2017; Lorrain et al., 2005; Takesue et al., 2008). A calcification rate control on Sr incorporation is also supported from abiogenic calcite (Gabitov et al., 2014) but not from abiogenic aragonite (Gabitov et al., 2006). Accordingly, this growth rate effect is probably of biologic nature in aragonite precipitates.

Sr probably arrives into the calcifying space via similar pathways to Ca, as was shown by the effects of calcium channel blockers in corals (Ferrier-Pagès et al., 2002). However, Ca-ATPase has a higher affinity for Ca (Yu and Inesi, 1995). Therefore, a higher Ca-ATPase activity, as a result of increased growth rates, should lead to decreasing Sr/Ca ratios in the precipitates, which was shown in corals (Ferrier-Pagès et al., 2002; de Villiers et al., 1995). As we expect high growth rates in the SRZ, Ca channels that also transport Sr cannot explain the observed Sr signature in this zone. Alternatively, the organisms metabolic rate has been suggested to control Sr/Ca in bivalves through metabolic pumping (Klein et al., 1996). High metabolic activity was observed in *A. excavata* infested by *H. sarcophaga,* indicated by a high concentration of nuclei, (Cedhagen, 1994). However, the model of Klein et al. would predict lower Sr/Ca ratios in these areas, thus a mechanism other than metabolic pumping must control the high Sr/Ca ratios in the SRZ.

Füllenbach et al. (2015) proposed that in slow growing areas of bivalves, the organisms exerts less biological control over element incorporation, leading to elevated Sr/Ca ratios. While this hypothesis does not fit our observation of elevated Sr/Ca ratios in a potentially fast growing shell area, a similar hypothesis was suggested concerning Mg/Ca in *Mytilus edulis* (Lorens and Bender, 1980). The authors found strongly elevated Mg/Ca ratios in shells sections that were precipitated after handling the specimens for size measurements and attributed this effect to stress (Lorens and Bender, 1980). The boring of *H. sarcophaga* is very likely to be a stress factor on *A. excavata*. An influence of such stress related effects on Mg/Ca and potentially Sr/Ca are, therefore, possible. The high Mg- concentrations in the EPF due to a potential breakdown of Mg-regulating mechanisms however, would inhibit the organism from calcification due to the inhibiting effects of Mg on crystal nucleation and growth (Lorens and Bender, 1980; Pytkowicz, 1965). *A. excavata* might circumvent this by releasing additional sulfate bearing organic molecules that provide additional nucleation sites and higher Ca- concentrations at the nucleation sites (Lorens and Bender, 1980), which we can observe by the increased S/Ca ratios in the SRZ.

5. Conclusion

https://doi.org/10.5194/bg-2021-74
Preprint. Discussion started: 29 March 2021

Our results demonstrate that the elemental and isotopic composition of the parasitic foraminifer *H. sarcophaga* varies depending on the host organisms that the foraminifer settles on. *H. sarcophaga* that lived on the coral *L. pertusa* shows significantly higher Sr/Ca ratios than those that lived on the bivalve *A. excavata*. Combining these data with a simple mixing model, we propose that this could point towards a biomineralization pathway that is influenced by uptake of carbonate material derived from the host. The dissolution of the host shell could serve to satisfy the foraminifers demand for calcium

We also observe significant differences between *H. sarcophaga* specimens that grew on *A. excavata* that can be correlated to the success of the penetration progress. Foraminifera that fully penetrated the bivalve's shell, recognizable by the hosts callus formation, display significantly lower Mn/Ca ratios than foraminifera that did not completely penetrate the shell. This could be an effect of a suspension feeding period of the foraminifera or grazing of Mn-rich material of the periostracum until it penetrated the bivalve's shell when switching to a parasitic mode of feeding. Other possibilities include differences in the growth rate caused by changes of the nutrient availability or Rayleigh fractionation.

The oxygen and carbon isotopic composition of *H. sarcophaga* also appears to be influenced by its specific host organism. Again, this might be an effect of a direct uptake of the host's organic material and/or $CaCO_3$ however other effects such as different pH regimes in the host organisms and varying equilibration may also play a role. Different extents of the calcification site carbonate system equilibration between HL and HA could also explain the missing signs of kinetic fractionation in HL compared to HA.

As the elemental and isotopic composition of some parasitic foraminifera is used for paleoceanographic reconstructions, our results clearly indicate that, if these findings are also applicable to other species, such studies should only be performed when the host organism and its chemical composition are known.

Author contribution

NS: Investigation**,** Conceptualization, Data curation, formal analysis, Investigation, Visualization, Writing (Original Draft)

DE: Methodology, Formal Analysis, Writing (Review & Editing)

MW: Resources**,** Writing (Review & Editing)

JVB: Resources, Writing (Review & Editing)

JF: Investigation, Resources, Writing (Review & Editing)

AF: Resources, Writing (Review & Editing)

https://doi.org/10.5194/bg-2021-74
Preprint. Discussion started: 29 March 2021

625 **SH:** Investigation, Writing (Review & Editing)

626 **HM:** Investigation, Resources, Writing (Review & Editing)

627 **SV:** Supervision, Resources, Writing (Review & Editing)

628 **JR:** Funding Acquisition, Project administration, Supervision, Resources, Writing (Review & Editing)

629 **Acknowledgments**

630 We are grateful to all cruise captains, crew members and cruise participants of research cruises
631 POS473 and POS525. We are also grateful for the help of Celestine Beyer and Luciano Zolezzi, who
632 aided with the measurements. This work was funded by the Deutsche Forschungsgemeinschaft, RA
633 2156-5/1 to JR. This is FIERCE contribution No. 70

634 **Supplements**

635 [1] Pictures of Meigen test

636 **Competing Interests**

637 The authors declare that they have no conflict of interest.

638 **References**

639 Addadi, L., Joester, D., Nudelman, F. and Weiner, S.: Mollusk Shell Formation : A Source of New
640 Concepts for Understanding Biomineralization Processes, , 980–987, doi:10.1002/chem.200500980,
641 2006.

642 Adkins, J. F., Boyle, E. A., Curry, W. B. and Lutringer, A.: Stable isotopes in deep-sea corals and a new
643 mechanism for "vital effects," Geochim. Cosmochim. Acta, 67(6), 1129–1143, doi:10.1016/S0016-
644 7037(02)01203-6, 2003.

645 Alexander, S. P. and Delaca, T. E.: Feeding adaptations of the foraminiferan Cibicides refulgens living
646 epizoically and parasitically on the Antarctic scallop Adamussium colbecki, Biol. Bull.,
647 doi:10.2307/1541868, 1987.

648 Allen, J. A.: Manganese deposition on the shells of living molluscs, Nature, doi:10.1038/185336b0,
649 1960.

650 Allen, K. A., Hönisch, B., Eggins, S. M., Haynes, L. L., Rosenthal, Y. and Yu, J.: Trace element proxies for
651 surface ocean conditions: A synthesis of culture calibrations with planktic foraminifera, Geochim.
652 Cosmochim. Acta, 193, 197–221, doi:10.1016/j.gca.2016.08.015, 2016.

653 Bajnai, D., Fiebig, J., Tomašových, A., Milner Garcia, S., Rollion-Bard, C., Raddatz, J., Löffler, N., Primo-

https://doi.org/10.5194/bg-2021-74
Preprint. Discussion started: 29 March 2021

654 Ramos, C. and Brand, U.: Assessing kinetic fractionation in brachiopod calcite using clumped
655 isotopes, Sci. Rep., 8(1), 533, doi:10.1038/s41598-017-17353-7, 2018.

656 Baranwal, S., Sauer, S., Knies, J., Chand, S., Jensen, H. and Klug, M.: Benthic foraminifera as tools in
657 interpretation of subsurface hydrocarbon fluid flow at Veslemøy High and Hola-Vesterålen areas of
658 the Barents Sea. [online] Available from:
659 https://ui.adsabs.harvard.edu/abs/2014EGUGA..16.1843B/abstract (Accessed 10 December 2020),
660 2014.

661 Beuck, L., López Correa, M. and Freiwald, A.: Biogeographical distribution of Hyrrokkin (Rosalinidae,
662 Foraminifera) and its host-specific morphological and textural trace variability, Curr. Dev. Bioerosion,
663 329–360, doi:10.1007/978-3-540-77598-0-17, 2008.

664 Bonucci, E. and Wheeler, A. P.: Mechanisms of Molluscan Shell Formation, in Calcification in
665 Biological Systems, pp. 179–216, Plenum Press., 2020.

666 Bromley, R. G. and Heinberg, C.: Attachment strategies of organisms on hard substrates: A
667 palaeontological view, Palaeogeogr. Palaeoclimatol. Palaeoecol., 232(2–4), 429–453,
668 doi:10.1016/j.palaeo.2005.07.007, 2006.

669 Büscher, J.: Cold-water coral habitat characterisation and in situ physiological state analyses of four
670 spatially distinct reefs in North- and mid-Norway ? Cruise Report RV POSEIDON 525 [POS525],
671 GEOMAR, Kiel, Germany., 2018.

672 Calvert, S. E. and Pedersen, T. F.: Geochemistry of Recent oxic and anoxic marine sediments:
673 Implications for the geological record, Mar. Geol., doi:10.1016/0025-3227(93)90150-T, 1993.

674 Calvert, S. E. and Pedersen, T. F.: Sedimentary geochemistry of manganese: Implications for the
675 environment of formation of manganiferous black shales, Econ. Geol.,
676 doi:10.2113/gsecongeo.91.1.36, 1996.

677 Carré, M., Bentaleb, I., Bruguier, O., Ordinola, E., Barrett, N. T. and Fontugne, M.: Calcification rate
678 influence on trace element concentrations in aragonitic bivalve shells: Evidences and mechanisms,
679 Geochim. Cosmochim. Acta, 70(19), 4906–4920, doi:10.1016/j.gca.2006.07.019, 2006.

680 Cedhagen, T.: Taxonomy and biology of hyrrokkin sarcophaga gen. Et Sp. N., a parasitic foraminiferan
681 (rosalinidae), Sarsia, 79(1), 65–82, doi:10.1080/00364827.1994.10413549, 1994.

682 Checa, A. G., Rodríguez-Navarro, A. B. and Esteban-Delgado, F. J.: The nature and formation of
683 calcitic columnar prismatic shell layers in pteriomorphian bivalves, Biomaterials, 26(32), 6404–6414,
684 doi:10.1016/j.biomaterials.2005.04.016, 2005.

https://doi.org/10.5194/bg-2021-74
Preprint. Discussion started: 29 March 2021

685 Chen, S., Gagnon, A. C. and Adkins, J. F.: Carbonic anhydrase, coral calcification and a new model of
686 stable isotope vital effects, Geochim. Cosmochim. Acta, 236, 179–197,
687 doi:10.1016/j.gca.2018.02.032, 2018.

688 Cheng, Y. R. and Dai, C. F.: A bioeroding foraminifer, Hyrrokkin sarcophaga, on deepwater corals from
689 the South China Sea, Coral Reefs, 35(3), 901, doi:10.1007/s00338-016-1447-7, 2016.

690 Cohen, A. L.: Geochemical Perspectives on Coral Mineralization, Rev. Mineral. Geochemistry, 54(1),
691 151–187, doi:10.2113/0540151, 2003.

692 Costa, K. B., Cabarcos, E., Santarosa, A. C. A., Battaglin, B. B. F. and Toledo, F. A. L.: A multiproxy
693 approach to the climate and marine productivity variations along MIS 5 in SE Brazil: A comparison
694 between major components of calcareous nannofossil assemblages and geochemical records,
695 Palaeogeogr. Palaeoclimatol. Palaeoecol., 449, 275–288, doi:10.1016/j.palaeo.2016.02.032, 2016.

696 Crenshaw, M. A.: The Inorganic Composition Of Molluscan ExtrapallialL Fluid, Biol. Bull., 143(3), 506–
697 512, doi:10.2307/1540180, 1972.

698 Dupuy, C., Rossignol, L., Geslin, E. and Pascal, P. Y.: Predation of mudflat meio-macrofaunal
699 metazoans by a calcareous foraminifer, Ammonia tepida (Cushman, 1926), J. Foraminifer. Res., 40(4),
700 305–312, doi:10.2113/gsjfr.40.4.305, 2010.

701 Elderfield, H.: A biomineralization model for the incorporation of trace elements into foraminiferal
702 calcium carbonate, Earth Planet. Sci. Lett., 142(3–4), 409–423, doi:10.1016/0012-821X(96)00105-7,
703 1996.

704 Erez, J.: The Source of Ions for Biomineralization in Foraminifera and Their Implications for
705 Paleoceanographic Proxies, Rev. Mineral. Geochemistry, 54(1), 115–149, doi:10.2113/0540115,
706 2003.

707 Falini, G., Albeck, S., Weiner, S. and Addadi, L.: Control of Aragonite or Calcite Polymorphism by
708 Mollusk Shell Macromolecules, Science (80-.)., 271(5245), 67–69, doi:10.1126/science.271.5245.67,
709 1996.

710 Ferrier-Pagès, C., Boisson, F., Allemand, D. and Tambutté, E.: Kinetics of strontium uptake in the
711 scleractinian coral Stylophora pistillata, Mar. Ecol. Prog. Ser., 245(Milliman 1974), 93–100,
712 doi:10.3354/meps245093, 2002.

713 Form, A. U., Büscher, J. V., Hissmann, K., Flögel, S., Wisshak, M., Rüggeberg, A., Bannister, R., Kutti, T.,
714 Stapp, L., Bennecke, S., Küter, M., Nachtigall, K., Schauer, J. and Fenske, M.: RV POSEIDON Cruise
715 Report POS473 LORELEI II: LOphelia REef Lander Expedition and Investigation II, Tromsø – Bergen –

716 Esbjerg, 15.08. – 31.08. – 04.09.2014., 2015.

717 Freiwald, A. and Schönfeld, J.: Substrate pitting and boring pattern of Hyrrokkin sarcophaga
718 Cedhagen, 1994 (Foraminifera) in a modern deep-water coral reef mound, Mar. Micropaleontol.,
719 28(2), 199–207, 1996.

720 Füger, A., Konrad, F., Leis, A., Dietzel, M. and Mavromatis, V.: Effect of growth rate and pH on lithium
721 incorporation in calcite, Geochim. Cosmochim. Acta, 248, 14–24, doi:10.1016/j.gca.2018.12.040,
722 2019.

723 Füllenbach, C. S., Schöne, B. R., Shirai, K., Takahata, N., Ishida, A. and Sano, Y.: Minute co-variations
724 of Sr/Ca ratios and microstructures in the aragonitic shell of Cerastoderma edule (Bivalvia) – Are
725 geochemical variations at the ultra-scale masking potential environmental signals?, Geochim.
726 Cosmochim. Acta, 205, 256–271, doi:10.1016/j.gca.2017.02.019, 2017.

727 Gabitov, R. I., Cohen, A. L., Gaetani, G. A., Holcomb, M. and Watson, E. B.: The impact of crystal
728 growth rate on element ratios in aragonite: An experimental approach to understanding vital effects,
729 Geochim. Cosmochim. Acta, 70(18), A187, doi:10.1016/j.gca.2006.06.377, 2006.

730 Gabitov, R. I., Sadekov, A. and Leinweber, A.: Crystal growth rate effect on Mg/Ca and Sr/Ca
731 partitioning between calcite and fluid: An in situ approach, Chem. Geol., 367, 70–82,
732 doi:10.1016/j.chemgeo.2013.12.019, 2014.

733 García-Gallardo, Á., Grunert, P., Voelker, A. H. L., Mendes, I. and Piller, W. E.: Re-evaluation of the
734 “elevated epifauna” as indicator of Mediterranean Outflow Water in the Gulf of Cadiz using stable
735 isotopes (δ13C, δ18O), Glob. Planet. Change, 155, 78–97, doi:10.1016/j.gloplacha.2017.06.005, 2017.

736 Goldstein, J. I., Newbury, D. E., Michael, J. R., Ritchie, N. W. M., Scott, J. H. J. and Joy, D. C.: Scanning
737 electron microscopy and x-ray microanalysis., 2017.

738 Goldstein, S. T.: Foraminifera: A biological overview, in Modern Foraminifera., 1999.

739 Gray, W. R. and Evans, D.: Nonthermal Influences on Mg/Ca in Planktonic Foraminifera: A Review of
740 Culture Studies and Application to the Last Glacial Maximum, Paleoceanogr. Paleoclimatology, 34(3),
741 306–315, doi:10.1029/2018PA003517, 2019.

742 Greaves, M., Caillon, N., Rebaubier, H., Bartoli, G., Bohaty, S., Cacho, I., Clarke, L., Cooper, M., Daunt,
743 C., Delaney, M., DeMenocal, P., Dutton, A., Eggins, S., Elderfield, H., Garbe-Schoenberg, D., Goddard,
744 E., Green, D., Groeneveld, J., Hastings, D., Hathorne, E., Kimoto, K., Klinkhammer, G., Labeyrie, L., Lea,
745 D. W., Marchitto, T., Martínez-Botí, M. A., Mortyn, P. G., Ni, Y., Nuernberg, D., Paradis, G., Quinn, T.,
746 Rosenthal, Y., Russel, A., Sagawa, T., Sosdian, S., Stott, L., Tachikawa, K., Tappa, E., Thunell, R. and

https://doi.org/10.5194/bg-2021-74
Preprint. Discussion started: 29 March 2021

747 Wilson, P. A.: Interlaboratory comparison study of calibration standards for foraminiferal Mg/Ca
748 thermometry, Geochemistry, Geophys. Geosystems, 9(8), 1–27, doi:10.1029/2008GC001974, 2008.

749 Groeneveld, J. and Filipsson, H. L.: Mg/Ca and Mn/Ca ratios in benthic foraminifera: the potential to
750 reconstruct past variations in temperature and hypoxia in shelf regions, Biogeosciences, 10(7), 5125–
751 5138, doi:10.5194/bg-10-5125-2013, 2013.

752 Sen Gupta, B. K.: Modern Foraminifera., 2003.

753 Halloran, B. A. and Donachy, J. E.: Characterization of organic matrix macromolecules from the shells
754 of the antarctic scallop, Adamussium colbecki, Comp. Biochem. Physiol. -- Part B Biochem., 111(2),
755 221–231, doi:10.1016/0305-0491(94)00245-P, 1995.

756 Hancock, L. G., Walker, S. E., Pérez-Huerta, A. and Bowser, S. S.: Population Dynamics and Parasite
757 Load of a Foraminifer on Its Antarctic Scallop Host with Their Carbonate Biomass Contributions,
758 edited by G. J. Vermeij, PLoS One, 10(7), e0132534, doi:10.1371/journal.pone.0132534, 2015.

759 Hare, P. E.: Amino acid composition of some calcified proteins, Carnegie Inst. Washingt. Yearbk., 64,
760 223–232, 1965.

761 Hissmann, K. and Schauer, J.: Manned submersible „JAGO“, J. large-scale Res. Facil. JLSRF, 3,
762 doi:10.17815/jlsrf-3-157, 2017.

763 Holcomb, M., Cohen, A. L., Gabitov, R. I. and Hutter, J. L.: Compositional and morphological features
764 of aragonite precipitated experimentally from seawater and biogenically by corals, Geochim.
765 Cosmochim. Acta, 73(14), 4166–4179, doi:10.1016/j.gca.2009.04.015, 2009.

766 Holland, K., Eggins, S. M., Hönisch, B., Haynes, L. L. and Branson, O.: Calcification rate and shell
767 chemistry response of the planktic foraminifer Orbulina universa to changes in microenvironment
768 seawater carbonate chemistry, Earth Planet. Sci. Lett., 464, 124–134, doi:10.1016/j.epsl.2017.02.018,
769 2017.

770 Hönisch, B., Allen, K. A., Russell, A. D., Eggins, S. M., Bijma, J., Spero, H. J., Lea, D. W. and Yu, J.:
771 Planktic foraminifers as recorders of seawater Ba/Ca, Mar. Micropaleontol., 79(1–2), 52–57,
772 doi:10.1016/j.marmicro.2011.01.003, 2011.

773 Horton, T., Kroh, A., Ahyong, S., Bailly, N., Boyko, C. B., Brandão, S. N., Gofas, S., Hooper, J. N. A.,
774 Hernandez, F., Holovachov, O., Mees, J., Molodtsova, T. N., Paulay, G., Decock, W., Dekeyzer, S.,
775 Poffyn, G., Vandepitte, L., Vanhoorne, B., Adlard, R., Agatha, S., Ahn, K. J., Akkari, N., Alvarez, B.,
776 Anderberg, A., Anderson, G., Angel, M. V, Antic, D., Arango, C., Artois, T., Atkinson, S., Auffenberg, K.,
777 Baldwin, B. G., Bank, R., Barber, A., Barbosa, J. P., Bartsch, I., Bellan-Santini, D., Bergh, N., Bernot, J.,

https://doi.org/10.5194/bg-2021-74
Preprint. Discussion started: 29 March 2021

778 Berta, A., Bezerra, T. N., Bieler, R., Blanco, S., Blasco-Costa, I., Blazewicz, M., Bock, P., Bonifacino de
779 León, M., Böttger-Schnack, R., Bouchet, P., Boury-Esnault, N., Boxshall, G., Bray, R., Bruce, N. L.,
780 Cairns, S., Calvo Casas, J., Carballo, J. L., Cárdenas, P., Carstens, E., Chan, B. K., Chan, T. Y., Cheng, L.,
781 Christenhusz, M., Churchill, M., Coleman, C. O., Collins, A. G., Collins, G. E., Corbari, L., Cordeiro, R.,
782 Cornils, A., Coste, M., Costello, M. J., Crandall, K. A., Cremonte, F., Cribb, T., Cutmore, S., Dahdouh-
783 Guebas, F., Daly, M., Daneliya, M., Dauvin, J. C., Davie, P., De Broyer, C., De Grave, S., de Mazancourt,
784 V., de Voogd, N. J., Decker, P., Defaye, D., d'Hondt, J. L., Dippenaar, S., Dohrmann, M., Dolan, J.,
785 Domning, D., Downey, R., Ector, L., Eisendle-Flöckner, U., Eitel, M., Encarnação, S. C. d., Enghoff, H.,
786 Epler, J., Ewers-Saucedo, C., et al.: World Register of Marine Species (WoRMS), [online] Available
787 from: http://www.marinespecies.org, 2021.

788 Immenhauser, A., Schöne, B. R., Hoffmann, R. and Niedermayr, A.: Mollusc and brachiopod skeletal
789 hard parts: Intricate archives of their marine environment, Sedimentology, 63(1), 1–59,
790 doi:10.1111/sed.12231, 2016.

791 Jacobson, P.: Physical Oceanography of the Trondheimsfjord, Geophys. Astrophys. Fluid Dyn., 26(1–
792 2), 3–26, doi:10.1080/03091928308221761, 1983.

793 Jochum, K. P., Nohl, U., Herwig, K., Lammel, E., Stoll, B. and Hofmann, A. W.: GeoReM: A New
794 Geochemical Database for Reference Materials and Isotopic Standards, Geostand. Geoanalytical Res.,
795 29(3), 333–338, doi:10.1111/j.1751-908x.2005.tb00904.x, 2005.

796 Kato, K., Wada, H. and Fujioka, K.: The application of chemical staining to separate calcite and
797 aragonite minerals for micro-scale isotopic analyses, Geochem. J., 37(2), 291–297,
798 doi:10.2343/geochemj.37.291, 2003.

799 Klein, R. T., Lohmann, K. C. and Thayer, C. W.: Sr/Ca and 13C/12C ratios in skeletal calcite of Mytilus
800 trossulus: Covariation with metabolic rate, salinity, and carbon isotopic composition of seawater,
801 Geochim. Cosmochim. Acta, doi:10.1016/S0016-7037(96)00232-3, 1996.

802 Koho, K. A., de Nooijer, L. J. and Reichart, G. J.: Combining benthic foraminiferal ecology and shell
803 Mn/Ca to deconvolve past bottom water oxygenation and paleoproductivity, Geochim. Cosmochim.
804 Acta, 165, 294–306, doi:10.1016/j.gca.2015.06.003, 2015.

805 Lackschewitz, K. and Heinitz, M.: Research Vessel POSEIDON, J. large-scale Res. Facil. JLSRF, 1, 60–63,
806 doi:10.17815/jlsrf-1-62, 2015.

807 Lantz, B.: The impact of sample non-normality on ANOVA and alternative methods, Br. J. Math. Stat.
808 Psychol., 66(2), 224–244, doi:10.1111/j.2044-8317.2012.02047.x, 2013.

https://doi.org/10.5194/bg-2021-74
Preprint. Discussion started: 29 March 2021

809 Lear, C. H. and Rosenthal, Y.: Benthic foraminiferal Li/Ca: Insights into Cenozoic seawater carbonate
810 saturation state, Geology, 34(11), 985, doi:10.1130/G22792A.1, 2006.

811 Lorens, R. B.: Sr, Cd, Mn and Co distribution coefficients in calcite as a function of calcite precipitation
812 rate, Geochim. Cosmochim. Acta, 45(4), 553–561, doi:10.1016/0016-7037(81)90188-5, 1981.

813 Lorens, R. B. and Bender, M. L.: The impact of solution chemistry on *Mytilus edulis* calcite and
814 aragonite, Geochim. Cosmochim. Acta, 44(9), 1265–1278, doi:10.1016/0016-7037(80)90087-3, 1980.

815 Lorrain, A., Gillikin, D. P., Paulet, Y. M., Chauvaud, L., Le Mercier, A., Navez, J. and André, L.: Strong
816 kinetic effects on Sr/Ca ratios in the calcitic bivalve Pecten maximus, Geology, 33(12), 965–968,
817 doi:10.1130/G22048.1, 2005.

818 Mackensen, A. and Nam, S. Il: Taxon-specific epibenthic foraminiferal δ18O in the Arctic Ocean:
819 Relationship to water masses, deep circulation, and brine release, Mar. Micropaleontol., 113, 34–43,
820 doi:10.1016/j.marmicro.2014.09.002, 2014.

821 Marchitto, T. M., Curry, W. B., Lynch-Stieglitz, J., Bryan, S. P., Cobb, K. M. and Lund, D. C.: Improved
822 oxygen isotope temperature calibrations for cosmopolitan benthic foraminifera, Geochim.
823 Cosmochim. Acta, 130, 1–11, doi:10.1016/j.gca.2013.12.034, 2014.

824 Marin, F., Luquet, G., Marie, B. and Medakovic, D.: Molluscan Shell Proteins: Primary Structure,
825 Origin, and Evolution, Curr. Top. Dev. Biol., 80(November 2018), 209–276, doi:10.1016/S0070-
826 2153(07)80006-8, 2007.

827 McConnaughey, T. A.: Sub-equilibrium oxygen-18 and carbon-13 levels in biological carbonates:
828 Carbonate and kinetic models, Coral Reefs, 22(4), 316–327, doi:10.1007/s00338-003-0325-2, 2003.

829 Milzer, G., Giraudeau, J., Faust, J., Knies, J., Eynaud, F. and Rühlemann, C.: Spatial distribution of
830 benthic foraminiferal stable isotopes and dinocyst assemblages in surface sediments of the
831 Trondheimsfjord, central Norway, Biogeosciences, 10(7), 4433–4448, doi:10.5194/bg-10-4433-2013,
832 2013.

833 Moradian-Oldak, J., Addadi, L., Weiner, S. and Berman, A.: Tuning of Crystal Nucleation and Growth
834 by Proteins: Molecular Interactions at Solid-Liquid Interfaces in Biomineralization, Croat. Chem. Acta,
835 63(3), 539–544 [online] Available from: https://hrcak.srce.hr/137390 (Accessed 1 December 2020),
836 1990.

837 Mucci, A.: Manganese uptake during calcite precipitation from seawater: Conditions leading to the
838 formation of a pseudokutnahorite, Geochim. Cosmochim. Acta, 52(7), 1859–1868, doi:10.1016/0016-
839 7037(88)90009-9, 1988.

https://doi.org/10.5194/bg-2021-74
Preprint. Discussion started: 29 March 2021

840 Mucci, A. and Morse, J. W.: The incorporation of Mg 2+ and Sr 2+ into calcite overgrowths: influences
841 of growth rate and solution composition, Geochim. Cosmochim. Acta, 47(2), 217?33, 1983.

842 Nakahara, H.: Nacre Formation in Bivalve and Gastropod Molluscs, in Mechanisms and Phylogeny of
843 Mineralization in Biological Systems, pp. 343–350, Springer Japan, Tokyo., 1991.

844 Petersen, J., Barras, C., Bézos, A., La, C., De Nooijer, L. J., Meysman, F. J. R., Mouret, A., Slomp, C. P.
845 and Jorissen, F. J.: Mn/Ca intra- and inter-test variability in the benthic foraminifer Ammonia tepida,
846 Biogeosciences, 15(1), 331–348, doi:10.5194/bg-15-331-2018, 2018.

847 Pytkowicz, R. M.: Rates of Inorganic Calcium Carbonate Nucleation, J. Geol., 73(1), 196–199,
848 doi:10.1086/627056, 1965.

849 Raddatz, J., Rüggeberg, A., Margreth, S. and Dullo, W. C.: Paleoenvironmental reconstruction of
850 Challenger Mound initiation in the Porcupine Seabight, NE Atlantic, Mar. Geol., 282(1–2), 79–90,
851 doi:10.1016/j.margeo.2010.10.019, 2011.

852 Raddatz, J., Liebetrau, V., Rüggeberg, A., Hathorne, E., Krabbenhöft, A., Eisenhauer, A., Böhm, F.,
853 Vollstaedt, H., Fietzke, J., López Correa, M., Freiwald, A. and Dullo, W. C.: Stable Sr-isotope, Sr/Ca,
854 Mg/Ca, Li/Ca and Mg/Li ratios in the scleractinian cold-water coral *Lophelia pertusa*, Chem. Geol.,
855 352, 143–152, doi:10.1016/j.chemgeo.2013.06.013, 2013.

856 Raddatz, J., Rüggeberg, A., Flögel, S., Hathorne, E. C., Liebetrau, V., Eisenhauer, A. and Dullo, W. C.:
857 The influence of seawater pH on U/Ca ratios in the scleractinian cold-water coral Lophelia pertusa,
858 Biogeosciences, 11(7), 1863–1871, doi:10.5194/bg-11-1863-2014, 2014.

859 Raddatz, J., Nürnberg, D., Tiedemann, R. and Rippert, N.: Southeastern marginal West Pacific Warm
860 Pool sea-surface and thermocline dynamics during the Pleistocene (2.5–0.5 Ma), Palaeogeogr.
861 Palaeoclimatol. Palaeoecol., 471, 144–156, doi:10.1016/j.palaeo.2017.01.024, 2017.

862 Raitzsch, M., Duenas-Bohórquez, A., Reichart, G. J., De Nooijer, L. J. and Bickert, T. T.: Incorporation
863 of Mg and Sr in calcite of cultured benthic foraminifera: Impact of calcium concentration and
864 associated calcite saturation state, Biogeosciences, 7(3), 869–881, doi:10.5194/bg-7-869-2010, 2010.

865 Rathburn, A. E. and De Deckker, P.: Magnesium and strontium compositions of Recent benthic
866 foraminifera from the Coral Sea, Australia and Prydz Bay, Antarctica, Mar. Micropaleontol., 32(3–4),
867 231–248, doi:10.1016/S0377-8398(97)00028-5, 1997.

868 Schleinkofer, N., Raddatz, J., Freiwald, A., Evans, D., Beuck, L., Rüggeberg, A. and Liebetrau, V.:
869 Environmental and biological controls on Na/Ca ratios in scleractinian cold-water corals,
870 Biogeosciences, 16(18), 3565–3582, doi:10.5194/bg-16-3565-2019, 2019.

https://doi.org/10.5194/bg-2021-74
Preprint. Discussion started: 29 March 2021

871 Schöne, B. R., Zhang, Z., Jacob, D., Gillikin, D. P., Tütken, T., Garbe-Schönberg, D., McConnaughey, T.
872 and Soldati, A.: Effect of organic matrices on the determination of the trace element chemistry (Mg,
873 Sr, Mg/Ca, Sr/Ca) of aragonitic bivalve shells (*Arctica islandica*) - Comparison of ICP-OES and LA-ICP-
874 MS data, Geochem. J., 44(1), 23–37, doi:10.2343/geochemj.1.0045, 2010.

875 Schweizer, M., Bowser, S. S., Korsun, S. and Pawlowski, J.: Emendation of Cibicides antarcticus
876 (Saidova, 1975) based on molecular, morphological, and ecological data, J. Foraminifer. Res.,
877 doi:10.2113/gsjfr.42.4.340, 2012.

878 Secor, C. L., Mills, E. L., Harshbarger, J., Kuntz, H. T., Gutenmann, W. H. and Lisk, D. J.:
879 Bioaccumulation of toxicants, element and nutrient composition, and soft tissue histology of zebra
880 mussels (Dreissena polymorpha) from New York State waters, Chemosphere, doi:10.1016/0045-
881 6535(93)90224-S, 1993.

882 Segev, E. and Erez, J.: Effect of Mg/Ca ratio in seawater on shell composition in shallow benthic
883 foraminifera, Geochemistry, Geophys. Geosystems, 7(2), 1–8, doi:10.1029/2005GC000969, 2006.

884 Smith, P. B. and Emiliani, C.: Oxygen-isotope analysis of recent tropical pacific benthonic
885 foraminifera, Science (80-.)., doi:10.1126/science.160.3834.1335, 1968.

886 Spötl, C. and Vennemann, T. W.: Continuous-flow isotope ratio mass spectrometric analysis of
887 carbonate minerals, Rapid Commun. Mass Spectrom., 17(9), 1004–1006, doi:10.1002/rcm.1010,
888 2003.

889 Stephenson, A. E., Deyoreo, J. J., Wu, L., Wu, K. J., Hoyer, J. and Dove, P. M.: Peptides enhance
890 magnesium signature in calcite: Insights into origins of vital effects, Science (80-.)., 322(5902), 724–
891 727, doi:10.1126/science.1159417, 2008.

892 Sunda, W. G. and Huntsman, S. A.: Regulation of cellular manganese and manganese transport rates
893 in the unicellular alga Chlamydomonas, Limnol. Oceanogr., 30(1), 71–80,
894 doi:10.4319/lo.1985.30.1.0071, 1985.

895 Swinehart, J. H. and Smith, K. W.: Iron And Manganese Deposition In The Periostraca Of Several
896 Bivalve Molluscs, Biol. Bull., 156(3), 369–381, doi:10.2307/1540924, 1979.

897 Takesue, R. K., Bacon, C. R. and Thompson, J. K.: Influences of organic matter and calcification rate on
898 trace elements in aragonitic estuarine bivalve shells, Geochim. Cosmochim. Acta, 72(22), 5431–5445,
899 doi:10.1016/j.gca.2008.09.003, 2008.

900 Tambutté, E., Allemand, D., Zoccola, D., Meibom, A., Lotto, S., Caminiti, N. and Tambutté, S.:
901 Observations of the tissue-skeleton interface in the scleractinian coral Stylophora pistillata, Coral

https://doi.org/10.5194/bg-2021-74
Preprint. Discussion started: 29 March 2021

902 Reefs, 26(3), 517–529, doi:10.1007/s00338-007-0263-5, 2007.

903 Tribovillard, N., Algeo, T. J., Lyons, T. and Riboulleau, A.: Trace metals as paleoredox and
904 paleoproductivity proxies: An update, Chem. Geol., 232(1–2), 12–32,
905 doi:10.1016/j.chemgeo.2006.02.012, 2006.

906 de Villiers, S., Nelson, B. K. and Chivas, A.: Biological Control on Coral Sr/Ca and d18O
907 Reconstructions of Sea Surface Temperatures, Science (80-.)., 269, 1247–1249, 1995.

908 Wada, K.: Biomineralization in bivalve molluscs with emphasis on the chemical composition of the
909 extrapallial fluid, Mech. Miner. Invertebr. plants, 1976.

910 Wada, K. and Fujinuki, T.: Physiological regulation of shell formation in molluscs, I. Chemical
911 composition of extrapallial fluid, Bull. Natl. Pearl Res. Lab., 18, 2085–2110, 1974.

912 Walker, S. E., Hancock, L. G. and Bowser, S. S.: Diversity, biogeography, body size and fossil record of
913 parasitic and suspected parasitic foraminifera: A review, J. Foraminifer. Res., 47(1), 34–55,
914 doi:10.2113/gsjfr.47.1.34, 2017.

915 Whitney, N. M., Johnson, B. J., Dostie, P. T., Luzier, K. and Wanamaker, A. D.: Paired bulk organic and
916 individual amino acid δ15N analyses of bivalve shell periostracum: A paleoceanographic proxy for
917 water source variability and nitrogen cycling processes, Geochim. Cosmochim. Acta, 254, 67–85,
918 doi:10.1016/j.gca.2019.03.019, 2019.

919 Wilbur, K. M. and Saleuddin, A. S. M.: Shell Formation, in The Mollusca, pp. 235–287, Elsevier., 1983.

920 Yu, X. and Inesi, G.: Variable stoichiometric efficiency of Ca2+ and Sr2+ transport by the sarcoplasmic
921 reticulum ATPase, J. Biol. Chem., 270(9), 4361–4367, doi:10.1074/jbc.270.9.4361, 1995.

922 Zhang, C. and Zhang, R.: Matrix proteins in the outer shells of molluscs, Mar. Biotechnol., 8(6), 572–
923 586, doi:10.1007/s10126-005-6029-6, 2006.

924